View metadata, citation and similar papers at core.ac.uk

brought to you by CORE

provided by Repositório da Universidade Nova de Lisboa

João Falé de Carvalho Madeira

High Performance Single Carrier Schemes for Massive MIMO Systems

Dissertação para obtenção do Grau de Mestre em

Engenharia Electrotécnica e de Computadores

Orientador:	Rui Miguel Henriques Dias Morgado Dinis , Professor Associado com Agregação, Faculdade de Ciências e Tecnologia da Universidade Nova de Lisboa
Co-orientador:	João Francisco Martinho Lêdo Guerreiro, Professor Auxiliar, Universidade Autónoma de Lisboa

Júri

Presidente:	Dr. André Teixeira Bento Damas Mora - FCT/UNL
Arguente:	Dr. Luís Filipe Lourenço Bernardo - FCT/UNL
Vogal:	Dr. Rui Miguel Henriques Dias Morgado Dinis - FCT/UNL

FACULDADE DE CIÊNCIAS E TECNOLOGIA
UNIVERSIDADE NOVA DE LISBOA

Março, 2019

High Performance Single Carrier Schemes for Massive MIMO Systems

Copyright © João Falé de Carvalho Madeira, Faculty of Sciences and Technology, NOVA University of Lisbon.
The Faculdade de Ciências e Tecnologia and the Universidade NOVA de Lisboa have the right, perpetual and without geographical boundaries, to file and publish this dissertation through printed copies reproduced on paper or on digital form, or by any other means known or that may be invented, and to disseminate through scientific repositories and admit its copying and distribution for non-commercial, educational or research purposes, as long as credit is given to the author and editor.

Este documento foi gerado utilizando o processador (pdf)LaTeX, com base no template "novathesis" [1] desenvolvido no Dep. Informática da FCT-NOVA [2].
[1] https://github.com/joaomlourenco/novathesis [2] http://www.di.fct.unl.pt

Acknowledgements

O trabalho desenvolvido ao longo desta dissertação não teria sido possível sem o apoio da Faculdade de Ciências e Tecnologia e do Instituto de Telecomunicações. Gostaria de agradecer ao meu professor orientador Rui Dinis e ao meu co-orientador João Guerreiro por toda a ajuda e apoio que forneceram durante este processo de elaboração de dissertação, bem como à equipa docente e não docente do departamento de Engenharia Electrotécnica.

Gostaria de agradecer aos meus colegas de curso por toda a ajuda e companhia ao longo destes cinco anos e meio, desde Programação de Microprocessadores até aos últimos dias na sala de mestrado.

Por último quero agradecer aos meus pais, José Madeira e Célia Madeira, e ao meu irmão, Ricardo Madeira, por todo o apoio que me deram e que me continuarão a dar, e à minha namorada, Leonor Augusto, por tornar estes anos do curso nos mais felizes que podiam ser.

Abstract

As the demands for faster and cheaper telecommunication systems continue to grow, so to do the demands for more efficient and secure systems. There have been several solutions proposed, with the most commonly accepted ones employing Massive Multiple Input, Multiple Output (mMIMO), featuring large arrays of antennas. The downside of these systems lies mainly in the need for computationally heavy channel equalization algorithms and the high hardware requirements, namely due to the need of many Power Amplifiers (PAs), Analog-to-Digital Converters (ADCs) and Digital-to-Analog Converters (DACs). This work analyses receivers that can handle these downsides, beginning with the low complexity equalization receivers Maximal-Ratio Detector (MRD) and Equal-Gain Detector (EGD), that can lower the equalization's computation time. Then a Singular Value Decomposition (SVD) receiver is studied, with a proposed interleaving scheme to allow for equal performance on all streams, combined with a scheme for estimating and cancelling the non-linear distortion to reduce the impact of cheaper and more power-efficient PAs. These receivers are then improved with the introduction of an error correcting convolutional code. Lastly, it is demonstrated that the SVD receiver can be appealing as a solution for Physical Layer Security (PLS) in mMIMO systems.

Keywords: Massive MIMO, Singular Value Decomposition, Physical Layer Security, Non-linearities.

Resumo

À medida que a procura por sistemas de telecomunicações mais rápidos e baratos aumenta, também aumenta a procura por sistemas mais eficientes e seguros. Dentro das várias soluções propostas, as mais consensuais consideram esquemas mMIMO, onde o número de antenas envolvido pode ser muito elevado. A desvantagem destes sistemas está principalmente na necessidade de algoritmos de igualização de canal de elevada complexidade, e também no requisito de muitos PAs, ADCs e DACs. Esta dissertação analisa receptores que conseguem lidar com estas desvantagens, começando pelos receptores de baixa complexidade de igualização MRD e EGD, que atingem um tempo de computação mais baixo.Foi também analisado um receptor baseado em SVD, com um esquema de *interleaving* para permitir que os diferentes fluxos tenham o mesmo desempenho. Este receptor foi combinado com um esquema onde se estima a distorção não-linear para reduzir o impacto de PAs mais baratos e energeticamente eficientes. Estes receptores são depois melhorados através de um código corretor de erros convolucional. Finalmente, demonstrou-se que o receptor SVD é uma solução interessante para PLS em sistemas mMIMO.

Palavras-chave: Massive MIMO, Decomposição em Valores Singulares, Segurança no Nível Físico, Não-linearidades.

Contents

List of Figures

Acronyms

16-QAM	16-Quadrature Amplitude Modulation.
4G	4th Generation.
5G	5th Generation.
64-QAM	64-Quadrature Amplitude Modulation.
ADC	Analog-to-Digital Converter.
AM/AM	Amplitude-to-Amplitude Modulation.
AM/PM	Amplitude-to-Phase Modulation.
APP	A Posteriori Probability.
AWGN	Additive White Gaussian Noise.
BER	Bit Error Rate.
BS	Base Station.
CSI	Channel State Information.
DAC	Digital-to-Analog Converter.
EGC	Equal-Gain Combining.
EGD	Equal-Gain Detector.
FDE	Frequency Domain Equalization.
FFT	Fast Fourier Transform.
GAMP	Generalised Approximate Message Passing.
GPRS	General Packet Radio Service.
GSM	Global System for Mobile Communications.
IB-DFE	Iterative Block - Decision Feedback Equalizer.

IFFT	Inverse Fast Fourier Transform.
IMP	Inter-Modulation Product.
IoT	Internet-of-Things.
IP	Internet Protocol.
ISI	Inter-Symbol Interference.
LDPC	Low-Density Parity-Check.
LLR	Log-likelihood Ratio.
LoS	Line-of-Sight.
LTE	Long Term Evolution.
MIMO	Multiple Input, Multiple Output.
MMSE	Minimum Mean Square Error.
M-QAM	M-ary Quadrature Amplitude Modulation.
mMIMO	Massive Multiple Input, Multiple Output.
MRC	Maximum-Ratio Combining.
MRD	Maximal-Ratio Detector.
MSE	Mean Squared Error.
MT	Mobile Terminal.
OFDM	Orthogonal Frequency-Division Multiplexing.
OSI	Open Systems Interconnection.
PA	Power Amplifier.
PAPR	Peak-to-Average Power Ratio.
PDF	Probability Density Function.
PHY	Physical Layer.
PLS	Physical Layer Security.
PSD	Power Spectral Density.
QAM	Quadrature Amplitude Modulation.
QoS	Quality of Service.
QPSK	Quadrature Phase Shift Keying.
SC	Single Carrier.
SC-FDE	Single Carrier with Frequency Domain Equalization.
SCR	Secrecy Rate.

SISO	Single Input, Single Output.
SNDR	Signal-to-Noise plus Distortion Ratio.
SNR	Signal-to-Noise-Ratio.
SR	Shift Register.
SSPA	Solid State Power Amplifier.
SVD	Singular Value Decomposition.
TDD	Time Division Duplexing.
ZF	Zero Forcing.

Chapter 1

Introduction

1.1 Scope and Motivation

In order to transmit knowledge between two people a form of communication is necessary. The simplest form of communication is often referred to as non-verbal communication, and it is not exclusive to humans. This technique is very limited in the amount of information it can transmit, but it fulfils the basic purpose of knowledge transmission between two entities. To increase the amount of information that can be transmitted, humanity started coding certain pieces of information as words, leading to the so-called verbal communication. This formed the basis for the different languages spoken throughout the world. This form of communication required all participants to be within range to listen to each other, which made it impossible to disseminate knowledge to large groups of people. The invention of the printing press brought a revolution that enabled the use of written communication, thereby removing the temporal and spatial constraints (to a degree) of communication between two people. The methods for knowledge transmission developed afterwards, such as books, letters and newspapers, would form the basis of knowledge transmission for millennia.

The discovery of electromagnetism by James Maxwell in the 19th century, and the confirmation of Maxwell's theory by Heirich Hertz 22 years later, ushered in the era of wireless communications. At first only simple signals could be transmitted, utilizing the same alphabet as the telegraph. It was not until the following century that it became possible to convert sound into high frequency electromagnetic waves to be sent over large distances. This type of wave was easier to transmit over large distances, in addition, they could use the air as a medium, which meant that the only necessary infrastructure was the transmitter and the receiver. This marked the beginning of mobile networks. Although it was possible to broadcast someone's voice over a large area, the rate of information

was still lower than paper based mediums. Transmitting the contents of a book could be much slower than handing the book to the intended receiver.

In 1948 Shannon proposed his theory of communication [1], where he demonstrated that any discrete system could achieve a Bit Error Rate (BER) as low as desired. In his work, Shannon developed a systematic approach for studying any discrete communication system, including languages, and determine how many bits must be transmitted by a discrete signal source. This theory, combined with switching circuits that used transistors invented in the previous year, allowed for the storage and replication of information without loss and in great part enabled the digital revolution. The analog communication systems of the time, including the existing first generation mobile networks, also began a slow shift into the digital domain, with the goal being to maximise the information encoded in one or more symbols, which can also be regarded as decreasing the number of bits that must be transmitted. This goal remains true in today's systems.

It was during the second generation of mobile networks that a new trend of offering services and content on mobile terminals started. Although the existing network Global System for Mobile Communications (GSM) already allowed access to the internet, it was very costly and impractical since the billing was done by connection duration. This meant that when web browsing the time between finishing and starting to load a new page was being billed, or before each page load a thirty second connection setup time was necessary. It was with the General Packet Radio Service (GPRS) that mobile data became more widespread. This technology came as an upgrade to the existing GSM and its main change from the old system was the replacement of circuit switching technology with packet switching. A new network core was created to operate with Internet Protocol (IP) packets, which greatly simplified the connection with outside networks, and billing now relied on the amount and size of the packets that the user sent/received, which enabled the usage of prepaid cards. In this network, users could reliably connect to the Internet and download content to their mobile device with easy to understand billing plans. However, users had faster connections at home with their modems, which led to a demand in higher internet access speeds on mobile networks. The following generations would focus on offering substantially higher data rates to users.

Telecommunication systems in the current generation (also denoted as 4th Generation (4G) or Long Term Evolution (LTE)) are no longer defined as voice services, but rather as high speed data and content delivery services ranging from instant messaging to high resolution streaming. All these different services impose ever higher requirements of the systems that deliver them to users, therefore elevating the need for systems that can surpass current technology. One of the main driving forces behind wireless communication are smartphones, which, thanks to their increasingly higher computing power, provide access to services and content to users at anytime and anyplace. The next generation, referred to as the 5th Generation (5G), will require higher data rates than its predecessor, however, due to the high cost of deploying an entirely new network, there will have to be a soft transition between generations. As an example, LTE introduced Multiple Input,

Multiple Output (MIMO) configurations, with higher orders being introduced in later releases. 5G will, therefore, further increase the number of antennas, entering what is referred to as Massive Multiple Input, Multiple Output (mMIMO).

As mobile devices achieved higher data rates, Quality of Service (QoS) and accessibility, they have become increasingly more common. To support this increasing number of mobile devices operators have had to increase the scale of their infrastructure, which in turn has to lead to more and more energy being consumed by the core network. In 2011, [2], researchers predicted that the radio access networks' energy consumption would remain constant over the years. In 2017 however, radio access networks consumed 65% of Vodafones global energy bill [3]. The usage of mm waves will require faster amplifiers, which will in turn draw more current to operate at such high frequencies. This fact, coupled with the data rate demands of 5G systems, means that the need for energy efficient receivers is now greater than ever.

1.2 Objectives

5G targets higher data rates and better QoS while maximising the information being transmitted and energy efficiency. However, there is a new demand in integrating devices other than smartphones, so called Internet-of-Things (IoT) devices, into the network. The demands of these devices vary greatly between types of devices. To that end, there are several new technologies being proposed at different layers, such as more efficient cores, less centralized signalling and even techniques that work across different layers. In this dissertation we will focus on the Physical Layer (PHY).

The first goal of this work is to increase the spectral and power efficiency of current systems. To that end, mMIMO techniques are used on Single Carrier with Frequency Domain Equalization (SC-FDE) systems, due to their lower envelope fluctuations when compared to Orthogonal Frequency-Division Multiplexing (OFDM), and introduce low complexity iterative receivers as a way to keep overall system complexity down. To further increase the energy efficiency of our system, we employ highly non-linear amplifiers combined with Singular Value Decomposition (SVD) receivers that can estimate and cancel the non-linear distortion. As security is also a very important requirement of 5G systems, we analyse the Physical Layer Security (PLS) performance of the proposed SVD system.

1.3 Main Contributions

The work developed in this dissertation has been published in [45] and [46], and there is still one additional conference paper, and two journal papers awaiting review.

1.4 Thesis Organisation

This dissertation is organised into four main chapters. Chapter 2 describes traditional single carrier systems in both Single Input, Single Output (SISO) and MIMO scenarios, and introduces advantages and disadvantages of these schemes. In chapter 3, different receiver implementations that allow lower complexity and delays at the cost of more transmission power, and a receiver that offers the opposite, i.e., less transmission power, but higher complexity are presented. In chapter 4, a security analysis of the receiver presented in the previous chapter in different scenarios is presented. Chapter 5 concludes this dissertation.

Chapter 2

State-of-Art

2.1 Goals of 5G Systems

As discussed in the previous chapter, the main force behind research in mobile telecommunications are the global mobile network systems used by the already immense and growing number of mobile subscribers. As the number of users grows, so too do the demands for a faster and better system that far exceeds the capabilities of current technology. Among these demands lie a tenfold increase in data rates as well as a maximum latency of 1 millisecond. These demands result in very high demands for the hardware and the algorithms employed.

In order to achieve these new requirements, several technologies are being proposed. In [4] a few possible approaches are studied. The first technique described proposes a new architecture for mobile networks, abandoning the traditional cell-based one. In the current architecture, a Mobile Terminal (MT) connects to a Base Station (BS) and proceeds to send information through an uplink channel and receive other information through a downlink channel. In order to secure these channels, other downlink and uplink control channels are first employed. This is what is referred to as a centralized approach. Due to the higher data rates and lower delay demands, the BS will need significantly higher processing power, making BSs much more expensive. In order to keep costs down, distributed approaches are being considered, such as introducing new long range stations to administer the control plane, separating it from the data plane, and other techniques that shift the processing to the MTs.

The frequency spectrum at the frequencies currently employed in mobile communications is being used to its limit, therefore, increasing data rates by increasing the bandwidth is not viable. However, a new interest for new carrier frequencies has surfaced,

particularly microwave frequencies within 3 to 300 GHz. Within this range of frequencies there are few that are licensed, allowing operators to reserve large bandwidths and, therefore, increase data rates. The main drawback of this approach lies in the hardware, as transmitters capable of operating with these frequencies are still very expensive.

Given the recent advancements in MT technology it is now interesting to discuss the possibility of smarter MTs. These MTs would be capable of performing more complex operations to reduce the stress on the network, such as being able to communicate directly with other MTs, caching non-priority traffic based on the network load, and computing more advanced algorithms to reduce channel interference.

The last approach, and the one that is the object of study in this dissertation, is the use of mMIMO systems. This type of system employs several antennas in both the BS and the MTs, which can offer many benefits. The most iconic benefit to mMIMO is the higher maximum data rate, although there are other benefits such as beamforming and combining [5]. This chapter will introduce classical single-carrier systems and iterative receivers, and analyse the costs and benefits of mMIMO systems. In addition, the advantages and drawbacks of mMIMO systems are analyzed.

2.2 Single Carrier Systems

2.2.1 Characterization

Let us consider a Single Carrier (SC) system that transmits N symbols, over a channel of bandwidth B, where the symbol duration is T_u. The complex envelope can be defined as

$$s_{sc}(t) = \sum_{m=0}^{m=N-1} s_m r(t - mT_u), \tag{2.1}$$

where s_n is the nth transmitted symbol and $r(t)$ denotes the support impulse, which is defined as

$$r(t) = \frac{1}{T_u} \operatorname{sinc}\left(\frac{t}{T_u}\right). \tag{2.2}$$

This impulse is chosen for two reasons. The first is that it guarantees no Inter-Symbol Interference (ISI) if it is sampled perfectly at every T_u instant. The second is due to its frequency response being defined as

$$R(f) = \operatorname{rect}(f T_u), \tag{2.3}$$

which maximises the occupied bandwidth. Since we use an optimum receiver, we require a detection filter with an impulse response equal to the support impulse. However, building a brick-wall filter in the frequency-domain is exceedingly difficult and costly, so a raised-cosine filter is used in real systems. This filter can occupy up to double the bandwidth of the ideal filter, but it is much simpler to build. In this work we consider the ideal filter.

The symbols depend on the modulation employed, for simplicity's sake we will first define the receiver for Quadrature Phase Shift Keying (QPSK), and then generalize for M-ary Quadrature Amplitude Modulation (M-QAM). The symbols to be transmitted are then defined as

$$\Re\mathfrak{e}(s_n) = \begin{cases} 1, & b_{2m} = 1 \\ -1, & b_{2m} = 0 \end{cases} \quad \mathfrak{Im}(s_n) = \begin{cases} 1, & b_{2m+1} = 1 \\ -1, & b_{2m+1} = 0 \end{cases}, \tag{2.4}$$

where b_m is the mth transmitted bit. The complex envelope $s_{sc}(t)$ can be expressed in the frequency domain as

$$S_{sc}(f) = \sum_{m=-\frac{N}{2}}^{m=\frac{N}{2}} S_n R(f) e^{-jmT_u 2\pi f}, \tag{2.5}$$

with S_n and $R(f)$ being the frequency domain counterpart of s_n and $r(t)$, respectively. The symbols are then convoluted with the channel considered and arrive at the receiver.

In standard SC transmission, the equalization is done in the time-domain. This process can be very complicated, especially when the delay spread of the channel is large. However, by using Frequency Domain Equalization (FDE), the equalization process can be greatly simplified.

2.2.2 Frequency Domain Equalization

Systems that employ time domain equalization are not suitable for highly time-dispersive channels. To mitigate this problem we employ FDE, seen in [6]. Let us consider a perfect receiver capable of perfectly estimating the channel between sender and receiver, with this channel being frequency-selective and perfectly estimated by the receiver. A block of symbols can be defined as

$$\mathbf{s} = [s_0, s_1, ...s_{N-1}], \tag{2.6}$$

with the symbols defined in (2.4), and a frequency counterpart obtained by computing the Fast Fourier Transform (FFT) of the block as

$$\mathbf{S} = [S_0, S_1, ...S_{N-1}]. \tag{2.7}$$

The considered frequency-selective channel is defined as

$$\mathbf{H} = [H_0, H_1, ..., H_{N-1}] \tag{2.8}$$

where H_k is the frequency response associated to the kth subcarrier, assuming that the channel is flat in the vicinity of the subcarrier. Regarding the frequency-domain, the received signal on the kth subcarrier can be written as

$$Y_k = H_k S_k + N_k, \tag{2.9}$$

with N_k denoting the Additive White Gaussian Noise (AWGN) component associated with the kth subccarier with zero-mean and one-sided Power Spectral Density (PSD) N_0. In

order to remove the channel from the received signal, the receiver obtains the equalized signal in a given subcarrier as

$$\tilde{S}_k = \frac{Y_k}{H_k}, \tag{2.10}$$

This constitutes the so-called Zero Forcing (ZF) equalization. As is widely known, the performance of this equalization process can be very low, since in the presence of strong deep fades, the noise can be substantially enhanced. In order to avoid noise enhancement, the equalized signal can be computed as

$$\tilde{S}_k = \frac{Y_k H_k^H}{|H_k|^2 + \frac{1}{SNR}}, \tag{2.11}$$

with SNR being the Signal-to-Noise-Ratio (SNR), assumed constant for the entire block. This method is called Minimum Mean Square Error (MMSE) due to prioritizing the minimum mean square error of the entire block and can achieve better performance than (2.10). After obtaining the equalized symbols, the receiver then converts the estimates to the time domain by using the Inverse Fast Fourier Transform (IFFT) as

$$\tilde{\mathbf{s}} = [\tilde{s}_1, \tilde{s}_2, .., \tilde{s}_N], \tag{2.12}$$

with $\tilde{\mathbf{s}}$ corresponding to the equalized received block. The equalized symbols are not binary values, as defined in (2.6), so a decision process is needed. The simplest decision method consists of defining a threshold that is equally distant between all possible values of $\mathbf{s}$, which in this case can be 0. The decisions are then computed as

$$\hat{b}_m = \begin{cases} 1, & \Re\mathfrak{e}(\tilde{s}_n) \geq 0 \\ 0, & \Re\mathfrak{e}(\tilde{s}_n) \leq 0 \end{cases} \quad \hat{b}_{m+1} = \begin{cases} 1, & \mathrm{Im}(\tilde{s}_n) \geq 0 \\ 0, & \mathrm{Im}(\tilde{s}_n) \leq 0 \end{cases}, \tag{2.13}$$

with $\tilde{s}_n$ being the nth equalized symbol, and $\hat{b}_m$ the mth estimated bit.

Since the symbols are estimated in the time domain and the equalization is made in the frequency-domain, it is possible to convert the decided symbols back to the frequency-domain in order to improve our equalization through nonlinear equalization processes. This process can be done iteratively and it is referred to as Iterative Block - Decision Feedback Equalizer (IB-DFE) in [7].

2.2.3 Iterative Block - Decision Feedback Equalizer

After obtaining the equalized symbols by computing (2.4), the hard-decisions can be computed as

$$\Re\mathfrak{e}(\hat{s}_n) = \begin{cases} 1, & \hat{b}_{2n} = 1 \\ -1, & \hat{b}_{2n} = 0 \end{cases} \quad \mathrm{Im}(\hat{s}_n) = \begin{cases} 1, & \hat{b}_{2n+1} = 1 \\ -1, & \hat{b}_{2n+1} = 0 \end{cases}, \tag{2.14}$$

and

$$\hat{\mathbf{s}} = [\hat{s}_0, \hat{s}_1, ..., \hat{s}_{N-1}], \tag{2.15}$$

is the block of hard-decision symbols with a frequency-domain counterpart obtained by Fast Fourier Transform (FFT)

$$\hat{\mathbf{S}} = [\hat{S}_0, \hat{S}_1, ..., \hat{S}_{N-1}], \tag{2.16}$$

which is uncorrelated with $\tilde{S}_k$. This block can be used to improve the equalization process by feeding it back to the equalizer. The symbol estimate for the kth sub-carrier, at the ith iteration, can be obtained with

$$\tilde{S}_k = Y_k F_k^{(i)} - B_k^{(i)} \hat{S}_k^{(i-1)}, \tag{2.17}$$

where $F_k^{(i)}$ is the feedforward equalization matrix, which is defined for an MMSE equalization as

$$F_k^{(i)} = \frac{H_k^H}{|H_k|^2 + \frac{1}{SNR}}, \tag{2.18}$$

and $B_k^{(i)}$ is a feedback factor that can be easily deduced for optimum performance to be

$$B_k^{(i)} = F_k^{(i)} H_k - 1. \tag{2.19}$$

Since this process only relies on the previous estimate, it can be done iteratively in order to improve performance. However, in cases of low SNR the symbol estimates may not be reliable. As such, an additional parameter, $\rho^{(i)}$, can be defined as a reliability factor that expresses the likelihood that a block is correct. In order to obtain this likelihood, a different type of decisions called "soft" decisions are necessary.

2.2.4 IB-DFE with Soft Decisions

Soft decisions, as shown in [8], differ in that instead of deciding based on a threshold, the probability of a given bit being correct is calculated and used as a measure. The likelihood of a bit being correct can be obtained from the distance between the received symbol $\tilde{\mathbf{s}}_n$ and all possible symbols in (2.4). However, it is unlikely that a symbol is, in the case of QPSK, near the centre of the constellation. With that assumption, we can simplify the calculations and simply compute the distance between the received symbol and the closest symbol where the bit in question is different.

For this calculation, the statistical test of log likelihood is used, which expresses how likely one hypothesis is over its null, or in this case, how likely the received symbol is equal to 1 or 0. The symbol can be split into its imaginary and real parts, with the real part referring to the even bits and the imaginary part to the odd bits and we define the Log-likelihood Ratio (LLR) for each part as

$$LLR_{2m}^{(i)} = log(\frac{P(Re(\tilde{s}_n^{(i)})=1)}{P(Re(\tilde{s}_n^{(i)})=0}) \quad LLR_{2m+1}^{(i)} = log(\frac{P(Im(\tilde{s}_n^{(i)})=1)}{P(Im(\tilde{s}_n^{(i)})=0}) \ , \tag{2.20}$$

where LLR_m is the log likelihood ratio for the mth bit, inserted into the matrix

$$\mathbf{LLR}^{(i)} = [LLR_0^{(i)}, LLR_1^{(i)}, .., LLR_{2N-1}^{(i)}]. \tag{2.21}$$

Since the probabilities are given by exponentials, the LLR calculation can be simplified to

$$LLR_{2m}^{(i)} = \frac{2}{\sigma_i^2}\Re\mathfrak{e}(\tilde{s}_n^{(i)}) \quad LLR_{2m+1}^{(i)} = \frac{2}{\sigma_i^2}\Im\mathfrak{m}(\tilde{s}_n^{(i)}) \ , \tag{2.22}$$

where σ_i^2 is the distance between the estimate and the transmitted symbol defined as

$$\sigma_i^2 = \frac{1}{2}\mathbb{E}[|s_n^{(i)} - \tilde{s}_n^{(i)}|^2]. \tag{2.23}$$

Since the receiver does not know the transmitted symbol an approximation can be computed as

$$\sigma_i^2 = \frac{1}{2N}\sum_{m=0}^{N-1}|\hat{s}_n^{(i)} - \tilde{s}_n^{(i)}|^2, \tag{2.24}$$

where $\hat{\mathbf{s}}_n$ denotes the hard-decision symbol. When the resulting symbol estimates are equal to the hard decided symbols then the receiver cannot improve the estimates any further. In order to use the feedback defined in (2.17), a soft-modulation is employed to convert the LLRs that range from 0 to ∞ into values between -1 and 1, defined as

$$\tilde{s}_n^{(i)} = \tanh\left(\frac{LLR_{2m}^{(i)}}{2}\right) + j\tanh\left(\frac{LLR_{2m+1}^{(i)}}{2}\right), \tag{2.25}$$

with their frequency counterparts $\tilde{S}_k^{(i)}$. We can express the reliability of the nth symbol as

$$\rho_n^{(i)} = \tanh\left(\frac{|LLR_{2m}^{(i)}|}{2}\right) + j\tanh\left(\frac{|LLR_{2m+1}^{(i)}|}{2}\right), \tag{2.26}$$

and the reliability of the entire block as

$$\rho^{(i)} = \frac{1}{2N}\sum_{n=0}^{N-1}\rho_n^{(i)}. \tag{2.27}$$

The feedforward matrix is rewritten as

$$F_k^{(i)} = \frac{H_k^H}{(1-|\rho^{(i-1)}|^2)|H_k|^2 + \frac{1}{SNR}}, \tag{2.28}$$

with $\rho^{(0)} = 0$, and (2.17) can be rewritten with the soft symbol estimations as

$$\tilde{S}_k^{(i)} = Y_k F_k^{(i)} - B_k^{(i)}\tilde{S}_k^{(i-1)}. \tag{2.29}$$

In order to measure the performance of this receiver we performed Monte Carlo simulations of 1000 blocks of 256 symbols each. Each block was sent through a different channel realization that follows a Rayleigh distribution, with $I = 16$ uncorrelated fading rays. We observe in fig. 2.1 the BER of this receiver. The first iteration has the worst performance due to only employing a weak equalization, however, the performance increases substantially when the IB-DFE is employed. Only four iterations are necessary for the receiver to converge to the optimum solution that minimises the Mean Squared Error (MSE).

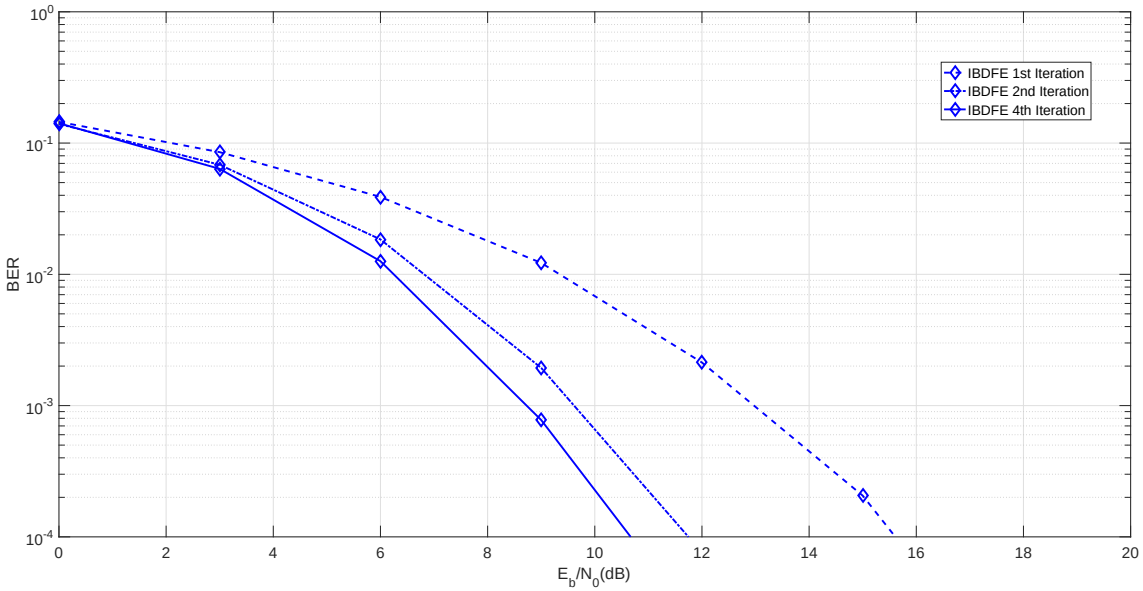

Figure 2.1: Simulated BER of the IB-DFE receiver.

2.2.5 Higher Order Modulations

Let us now examine the IB-DFE receiver for M-QAM constellations. We define the nth M-QAM symbol in a block as

$$\mathrm{Re}(s_n) = \sum_{m=n}^{n+\mu/2} 2^{\mu/2-m} \prod_{m'=n}^{m} b_{(m')} \tag{2.30}$$

$$\mathrm{Im}(s_n) = \sum_{m=n+\mu/2}^{n+\mu} 2^{\mu-m} \prod_{m'=n+\mu/2}^{m} b_{(m')}, \tag{2.31}$$

where $\mu = \log 2(M)$. For consistency, we will fix the block size at N, indexed by n, and for higher order modulations we will increase the number of bits per block to $\mu N = L$.

With the newly defined symbols we have to, likewise, redefine our LLR (2.20), soft modulation ((2.25)) and reliability (2.26) computations. We calculate the LLRs, according to [9], as

$$\begin{aligned} LLR_m^{(i)} = &\frac{1}{\sigma_i^2}(\mathrm{Re}(\tilde{s}_n^{(i)} - \hat{s}_n^1) + \mathrm{Im}(\tilde{s}_n^{(i)} - \hat{s}_n^1) \\ &- \mathrm{Re}(\tilde{s}_n^{(i)} - \hat{s}_n^0) + \mathrm{Im}(\tilde{s}_n^{(i)} - \hat{s}_n^0)), \end{aligned} \tag{2.32}$$

where $\hat{s}_n^1$ and $\hat{s}_n^0$ are the closest symbols to the received symbol with the bit in the mth position set to 1 and 0, respectively, and σ_i is as defined in 2.24. The soft modulation process is defined as

$$\mathrm{Re}(\bar{s}_n^{(i)}) = \sum_{m=1}^{\mu/2} 2^{\mu/2-m} \prod_{m'=0}^{m-1} \tanh\left(\frac{LLR_{(n+m')}^{(i)}}{2}\right), \tag{2.33}$$

and

$$\mathrm{Im}(\bar{s}_n^{(i)}) = \sum_{m=1}^{\mu/2} 2^{\mu/2-m} \prod_{m'=0}^{m-1} \tanh\left(\frac{LLR_{(n+m'+\mu/2)}^{(i)}}{2}\right). \tag{2.34}$$

To compute the block reliability factor we must first define the in-phase and quadrature bit reliabilities as

$$\rho_{n,I}^{(i)} = \sum_{m=1}^{\mu/2} 2^{\mu-2m} \prod_{m'=0}^{m-1} \tanh\left(\frac{|LLR_{(n+m')}^{(i)}|}{2}\right), \tag{2.35}$$

and

$$\rho_{n,Q}^{(i)} = \sum_{m=1}^{\mu/2} 2^{\mu-2m} \prod_{m'=0}^{m-1} \tanh\left(\frac{|LLR_{(n+m'+\mu/2)}^{(i)}|}{2}\right). \tag{2.36}$$

Under these conditions, the block reliability factor is defined as

$$\rho^{(i)} = \frac{\rho_{n,I}^{(i)} + \rho_{n,Q}^{(i)}}{4N\sigma_s^2}, \tag{2.37}$$

where σ_s^2 is the symbol variance given by

$$2\sigma_s^2 = \mathbb{E}[|s_n^2|]. \tag{2.38}$$

Employing a higher order modulation allows for higher spectral efficiency, as we are increasing the amount of information sent over the channel while maintaining the bandwidth restriction. However, the error probability for certain symbols in the constellation is larger when compared to QPSK. In QPSK, the symbol error probability is mainly conditioned by the two neighbouring symbols, while in 16-Quadrature Amplitude Modulation (16-QAM) symbols can have up to four equidistant neighbouring symbols, as shown in fig. 2.2, leading to an overall higher symbol error rate. If we consider 64-Quadrature Amplitude Modulation (64-QAM), then only four symbols out of 64 have 2 neighbours, with most symbols having four neighbours. As such, there is a larger performance degradation associated to using larger constellations.

Fig. 2.3 confirms this increased BER when larger constellations are employed. It shows the BER of an IB-DFE receiver when $N = 256, I = 16$ and different values of M are considered.

2.2.6 APP Decoding

As shown by Claude E. Shannon in 1949, [10], our telecommunication systems can achieve much lower BERs through the use of more efficient coding techniques. Since real world systems are bounded on the amount of power they can transmit, as well as typically being mobile devices with finite battery, error correcting coding techniques are implemented in order to increase efficiency. As seen in [11], the addition of an error correcting code can effectively multiply our system performance, although this is at the cost of higher bandwidth and complexity.

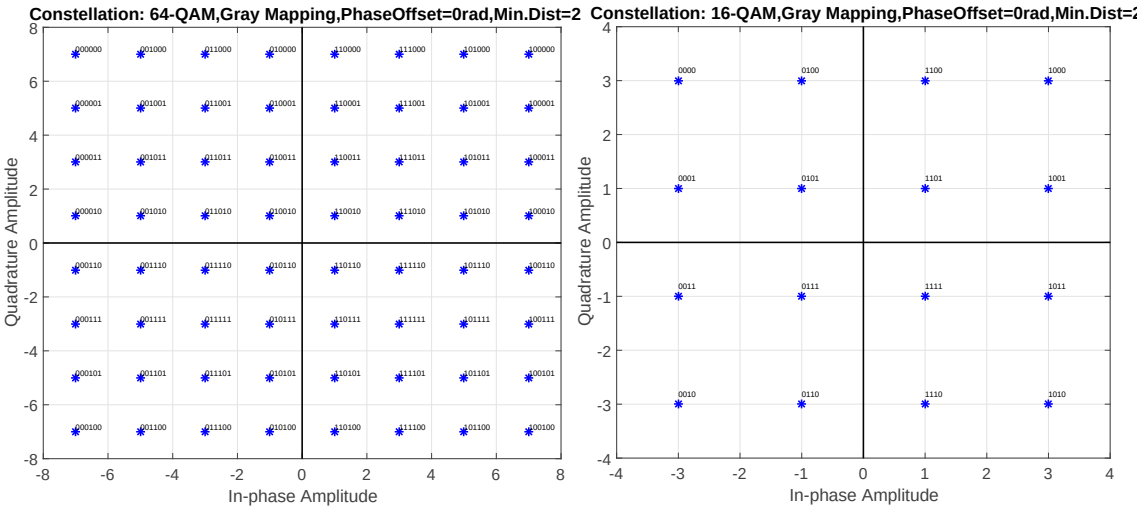

Figure 2.2: Constellation used for 16 and 64 Quadrature Amplitude Modulation (QAM).

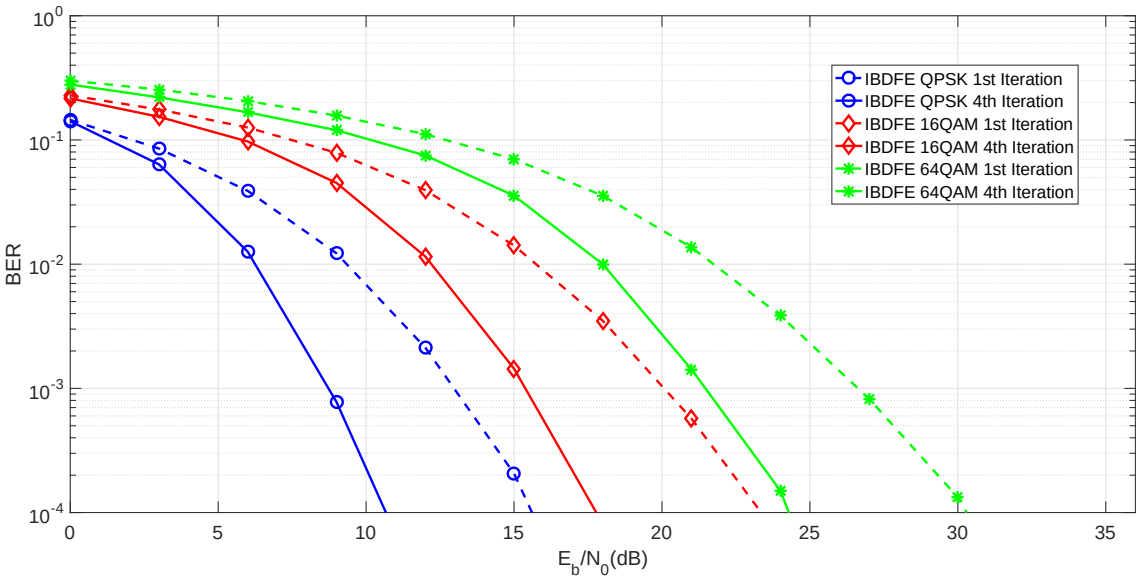

Figure 2.3: Comparison of the BER of the IB-DFE receiver for M-QAM constellations.

For this receiver, we will implement a conventional 64 states, 1/2 rate convolutional code, [12], which will greatly boost the performance of our system. This encoder's diagram is shown in fig. 2.4. For the decoder, we use a soft-in,soft-out A Posteriori Probability (APP) decoder, based on [13], which takes the LLRs of the received coded bits, and outputs the LLRs for the decoded bits. It also outputs the coded bit LLRs that are used in the IB-DFE feedback. There are more sophisticated and powerful codes, such as the Low-Density Parity-Check (LDPC) [14] and Turbo codes [15], however, these techniques are iterative, and would require more research on the optimum allocation of coding iterations with IB-DFE iterations.

In order to decode a received block, we first define the conditional probability of a certain state, given the received sequence of bits. Additionally, we define the conditional

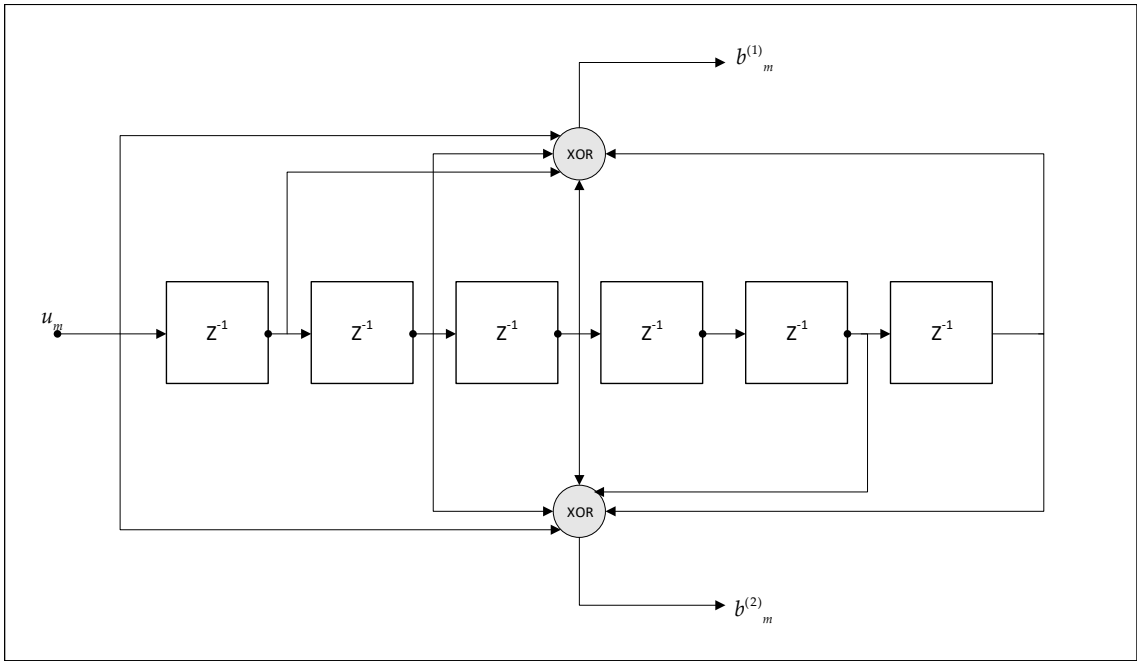

Figure 2.4: Diagram of the optimum 64 states 1/2 rate convolutional encoder.

probability of a certain state, and the previous state, for a given received sequence of bits. A given mth state is defined as

$$\mathbf{C}_m = [c_m^{(1)}, c_m^{(2)}, ..., c_m^{(CL)}], \tag{2.39}$$

where $c_m^{(1)}$ is the value stored in the first Shift Register (SR) for the mth input bit. With this definition, we write the conditional probabilities as

$$\Pr\{\mathbf{C}_m = \mathbf{p}|\tilde{\mathbf{b}}\} = \Pr\{\mathbf{C}_m = \mathbf{p}; \tilde{\mathbf{b}}\}/\Pr\{\tilde{\mathbf{b}}\}, \tag{2.40}$$

and

$$\Pr\{\mathbf{C}_{m-1} = \mathbf{p}'; \mathbf{C}_m = \mathbf{p}|\tilde{\mathbf{b}}\} = \Pr\{\mathbf{C}_{m-1} = \mathbf{p}'; \mathbf{C}_m = \mathbf{p}; \tilde{\mathbf{b}}\}/\Pr\{\tilde{\mathbf{b}}\}, \tag{2.41}$$

where $\mathbf{p}$ is one of the possible states of the code, with $\mathbf{p}'! = \mathbf{p}$, and $\tilde{\mathbf{b}}$ is the sequence of received bits of length $N \log 2(M)$. With our objective defined, we begin by defining the joint probabilities

$$\lambda_m(\mathbf{p}) = \Pr\{\mathbf{C}_m = \mathbf{p}; \tilde{\mathbf{b}}\}, \tag{2.42}$$

and

$$\sigma_m(\mathbf{p}', \mathbf{p}) = \Pr\{\mathbf{C}_{m-1} = \mathbf{p}'; \mathbf{C}_m = p; \tilde{\mathbf{b}}\}. \tag{2.43}$$

Since $\tilde{\mathbf{b}}$ is independent of the state $\mathbf{p}$, then $\Pr\{\tilde{\mathbf{b}}\}$ is constant. Thus we can divide (2.42) and (2.43) by $\Pr\{\tilde{\mathbf{b}}\}$, which is simply $\lambda_m(0)$, and obtain the conditional probabilities in (2.40) and (2.41).

We now define three auxiliary probability functions as

$$\alpha_m(\mathbf{p}) = \Pr\{\mathbf{C}_m = \mathbf{p}; \tilde{\mathbf{b}}_1^m\}, \tag{2.44}$$

$$\beta_m(\mathbf{p}) = \Pr\{\tilde{\mathbf{b}}_{m+1}^{L} | \mathbf{C}_m = \mathbf{p}\}, \tag{2.45}$$

$$\gamma_m(\mathbf{p}', \mathbf{p}) = \Pr\{\mathbf{C}_m = \mathbf{p}; \tilde{b}_m | \mathbf{C}_{m-1} = \mathbf{p}'\}, \tag{2.46}$$

where $\tilde{\mathbf{b}}_1^m$ and $\tilde{\mathbf{b}}_{m+1}^{L}$ refer to the first m and the last $L-m$ bit estimates, respectively. We use $\alpha_m(\mathbf{p})$ to represent the probability of the sequence of states from the start to the current state, $\beta_m(\mathbf{p})$ to represent the probability of the sequence states from the current to the last state. Both of these functions are computed recursively. $\gamma_m(\mathbf{p}', \mathbf{p})$ corresponds to the probability of going from state $\mathbf{p}'$ to state $\mathbf{p}$.

Using these functions, we expand (2.42) as

$$\begin{aligned} \lambda_m(\mathbf{p}) &= \Pr\{\mathbf{C}_m = \mathbf{p}; \tilde{\mathbf{b}}_1^m\} \cdot \Pr\{\tilde{\mathbf{b}}_{m+1}^{L} | \mathbf{C}_m = \mathbf{p}; \tilde{\mathbf{b}}_1^m\} \\ &= \alpha_m(\mathbf{p}) \cdot \Pr\{\tilde{\mathbf{b}}_{m+1}^{L} | \mathbf{C}_m = \mathbf{p}\} \\ &= \alpha_m(\mathbf{p}) \cdot \beta_m(\mathbf{p}). \end{aligned} \tag{2.47}$$

The second step, as explained in [13], comes from the Markov property that if C_m is known, then events after m do not depend on the input $\tilde{\mathbf{b}}_1^m$. Likewise, we can expand (2.43) as

$$\begin{aligned} \sigma_m(\mathbf{p}', \mathbf{p}) &= \Pr\{\mathbf{C}_{m-1} = \mathbf{p}'; \tilde{\mathbf{b}}_1^{m-1}\} \cdot \Pr\{\mathbf{C}_m = \mathbf{p}; \tilde{\mathbf{b}}_m | \mathbf{C}_{m-1} = \mathbf{p}'\} \cdot \Pr\{\tilde{\mathbf{b}}_{m+1}^{L} | \mathbf{C}_m = \mathbf{p}\} \\ &= \alpha_{m-1}(\mathbf{p}') \cdot \gamma_m(\mathbf{p}', \mathbf{p}) \cdot \beta_m(\mathbf{p}), \end{aligned} \tag{2.48}$$

where $\tilde{\mathbf{b}}_1^{m-1}$ are the first $m-1$ bit estimates.

We now define the set of states $\mathbf{C}_m$ where $c_m^{(1)} = 0$ as $\mathbf{A}$. The likelihood that a given bit will be decoded as a 0 is defined as

$$\Pr\{b_m = 0 | \tilde{\mathbf{b}}_m\} = \frac{1}{\lambda_m(0)} \sum_{\mathbf{p} \in \mathbf{A}} \lambda_m(\mathbf{p}). \tag{2.49}$$

Likewise, we define $\mathbf{B}^{(j)}$ as the set of transitions $\mathbf{C}_{m-1} = \mathbf{p}' \rightarrow \mathbf{C}_m = \mathbf{p}$ such that the jth output bit $u_m^{(j)}$ of a given uncoded bit is 0 as

$$\Pr\{u_m^{(j)} = 0; \tilde{\mathbf{b}}_m\} = \sum_{(\mathbf{p}', \mathbf{p}) \in \mathbf{B}^{(j)}} \sigma_m(\mathbf{p}', \mathbf{p}). \tag{2.50}$$

2.3 MIMO Systems

This type of system utilizes communications that rely on more than one antenna per MT or BS, with the MTs having T antennas and the BS with R antennas in the uplink scenario, and vice versa in the downlink. Under these conditions there are three common scenarios, as shown in Fig.2.5, which we will now describe in order left-to-right. The simplest case is a downlink transmission between the BS with T antennas, and a single MT with R antennas, and vice-versa for an uplink scenario. In the second scenario, we have a downlink transmission between a single BS with T antennas, and several MTs, each with R antennas, and in the last scenario we have an uplink transmission between several

MTs, each with T antennas, and a single BS with R antennas. These second and third scenarios introduce added complexity due to interference during channel estimation. For this analysis we will assume perfect Channel State Information (CSI), in order to better present the advantages of MIMO. The number of channels between MT and BS in these systems is therefore $T \times R$, which provides several possible benefits, although some with significant drawbacks [16]. Let us examine each of these.

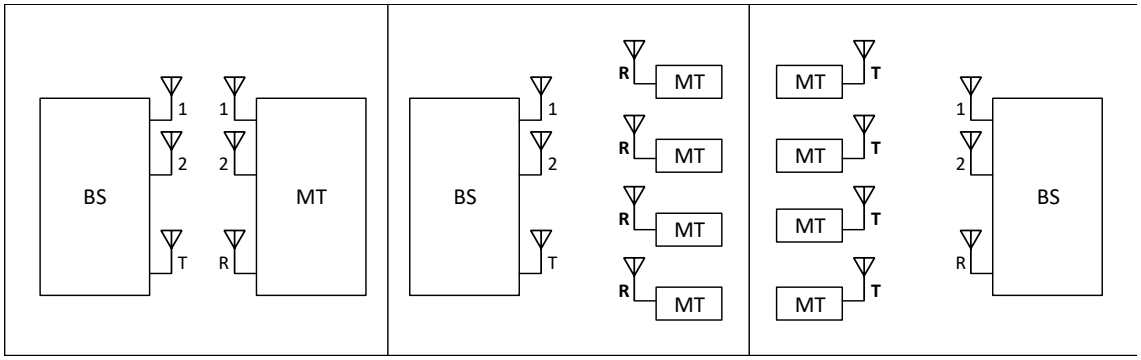

Figure 2.5: Diagram of three MIMO scenarios. On the left, a downlink transmission between a BS and an MT. In the middle, a downlink transmission between a BS and several MTs. On the right, an uplink transmission between several MTs and a BS. Bold symbols represent multiple antennas.

2.3.1 Benefits

There are several benefits introduced by a MIMO system, [17], starting with channel capacity. As described in [18], the maximum capacity of a fading channel can be increased by increasing the number of antennas. In the case of a Rayleigh Channel we have the MIMO capacity as

$$C_{T,R} = B\log\left(\det\left(\mathbf{I}_R + \frac{SNR}{T}\mathbf{H}\mathbf{H}^H\right)\right), \tag{2.51}$$

where B is the signal bandwidth, $\mathbf{I}_R$ is an identity matrix of rank R, which is the number of receiving antennas, T is the number of transmitting antennas, and $\mathbf{H}$ is the $T \times R$ channel matrix. We can use SVD to decompose $\mathbf{H}$ as

$$\mathbf{H} = \mathbf{U}\mathbf{\Lambda}\mathbf{V}^H, \tag{2.52}$$

where $\mathbf{U}$ and $\mathbf{V}^H$ are unitary matrices, and $\mathbf{\Lambda}$ is a diagonal matrix of size $\min(R,T)$ that contains the singular values of $\mathbf{H}$. With this decomposition, we rewrite the capacity as

$$C_{T,R} = \sum_{n=1}^{R_H} B\log(1 + \frac{SNR}{T}\lambda_n^2), \tag{2.53}$$

where λ_n is the nth singular value, and R_H is the number of non-zero singular values such that $R_H \leq \min(R,T)$. It is demonstrated in [19] that for $T >> R$, the capacity scales linearly with R, and for very high SNR, the capacity scales linearly with $\min(R,T)$. This means

the maximum data rate also increases linearly, leading to a large increase in performance, as described in [20].

A MIMO symbol at the nth time slot can be defined as

$$\mathbf{s}_n = [s_n^1, s_n^2, ..., s_n^{R_H}], \tag{2.54}$$

with its frequency-domain counterpart denoted by $\mathbf{S}_k$.

Since the transmission involves multiple data symbols, the number of channels also increased. The impulse response at the kth sub-carrier of the channel matrix is defined as

$$\mathbf{H}_k = \begin{bmatrix} H_k^{1,1} & H_k^{1,2} & \cdots & H_k^{1,T} \\ H_k^{2,1} & H_k^{2,2} & \cdots & H_k^{2,T} \\ \vdots & \vdots & \ddots & \vdots \\ H_k^{R,1} & H_k^{R,2} & \cdots & H_k^{R,T} \end{bmatrix}. \tag{2.55}$$

The received signal at the kth subcarrier is defined as

$$\mathbf{Y}_k = \mathbf{H}_k \mathbf{S}_k + \mathbf{N}_k. \tag{2.56}$$

Similarly, we define the equalization as

$$\tilde{\mathbf{S}}_k = \mathbf{Y}_k \mathbf{F}_k^{(i)} - \mathbf{B}_k^{(i)} \tilde{\mathbf{S}}_k^{(i-1)}. \tag{2.57}$$

Fig. 2.6 shows the BER of a MIMO system with $T = R = 32$, under the same simulation conditions as before. When comparing the results with the SISO system, we notice that the QPSK MIMO receiver performs better than the SISO receiver, although as we will see next it suffers from greatly increased complexity. On the other hand, the higher modulations perform worse under MIMO conditions. This is due to the channel interference between adjacent channels being aggravated by the non constant symbol power in these modulations.

2.3.2 Massive MIMO

When MIMO systems are expanded to employ very large antenna arrays, then we refer to them as mMIMO systems. The benefits from traditional MIMO systems are also present in mMIMO, augmented by the amount of antennas involved. However, mMIMO systems also aggravate the existing drawbacks of MIMO, to the point where it becomes infeasible to simply increase the antennas on existing systems. It is therefore necessary to look at the challenges that arise when designing mMIMO systems.

2.3.3 Channel Estimation and Equalization

In a SISO system, the receiver has to obtain the CSI for the equalization process. Between a given pair of antennas, the frequency response of this channel, as expressed in (2.8), can be characterized as a sequence of N sub-carriers, each considered flat in their bandwidth.

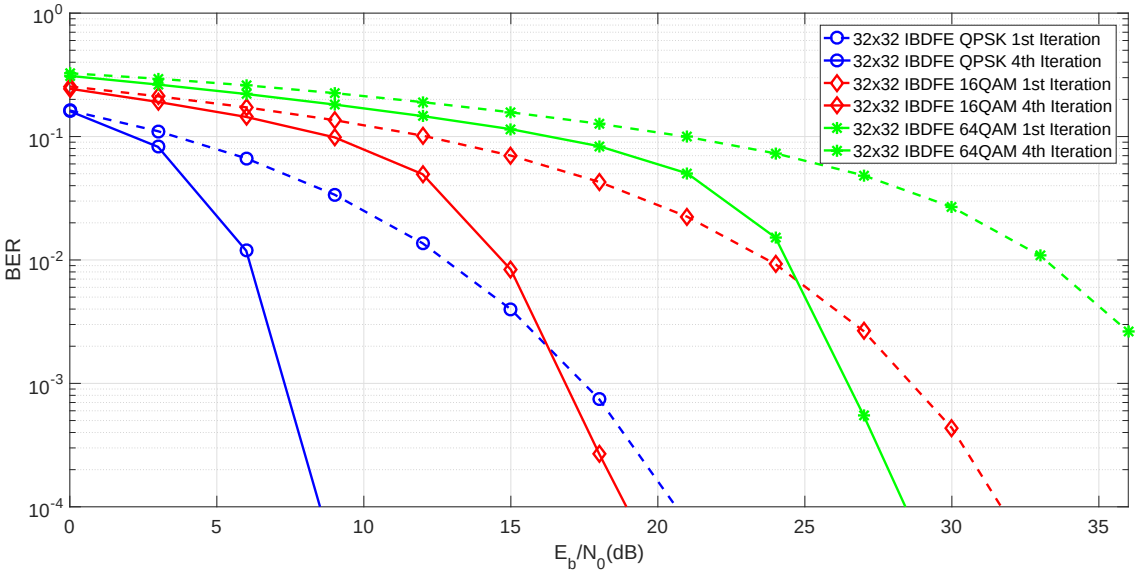

Figure 2.6: Comparison of the BER of the IB-DFE receiver for various modulations.

In order to estimate the channel, the transmitter sends a sequence of known symbols, referred to as pilots, which allows the receiver to obtain the channel impulse response by dividing the received frequency domain signal by the known pilot sequence.

In the case of a MIMO system however, the number of channels to estimate is given by $R \times T$, which in the case of a 2-by-2 system would mean 4 channels. If the transmitter sends the same pilot sequence in both antennas, then each antenna in the receiver would obtain a signal that is the sum of the two pilot sequences across two different channels. Therefore, the receiver can no longer divide the received signal by the pilots, as it would obtain the sum of the two channels. In order to separate the channels in the receiver, the sender uses two orthogonal pilot sequences, as described in [21], which can be chosen to have length 2, one for each antenna, that allow the receiver to properly separate each pilot sequence and thus differentiate the channels. However, we are now sending 4 times more pilots than the SISO system, and have gained only twice the data rate.

In mMIMO systems the number of channels to estimate grows exponentially with R and T, making channel estimation increasingly harder due to the requirement of orthogonal pilot sequences, since the length of the sequence must be equal to or greater than the number of receiving antennas, R. This requirement severely degrades the spectral efficiency as the number of antennas grows. There are several proposed pilot schemes, such as pilot patterns based on Kalman filtering [22], and schemes based on low numbers of observations such as [23], that attempt to minimise the necessary number of pilots for CSI estimation.

Further compounding the issue with channel estimation is the difficulty in performing channel equalization. Since the channel for a certain sub-carrier k, $\mathbf{H}_k$, is no longer a single value, but an entire matrix of size $R \times T$. As such, inverting the channel effect on that same sub-carrier requires inverting the matrix, as defined in (2.11), which is significantly

slower, and becomes worse with larger arrays of antennas. Since this results in a larger maximum delay, it is preferred to adopt receivers with lower complexity that can simplify these calculations.

2.3.4 Non-linearities

The techniques currently being proposed place a heavy burden on the hardware, which historically in mobile networks has tried to be as low-cost as possible. With this line of thinking, there is research being done into how to best use cheap electronics, such as saturated amplifiers [24], and low resolution Digital-to-Analog Converter (DAC)/Analog-to-Digital Converter (ADC) [25]. These components introduce non-linearities in the signals that can negatively impact performance.

2.3.4.1 Non-ideal ADC and DAC

When discussing the maximum performance of a system it is assumed that the transmitted signal is perfectly converted from the digital domain to the analog domain in the sender, and the inverse on the receiver. However, this is only the case if the modules in question, the DAC and ADC, have infinite bit resolution and an infinite linear dynamic range. An infinite bit resolution would mean that the converter can express analog values with infinite precision. In addition, the processor's memory would also have to be infinite to accommodate the infinite bits. Since we, obviously, cannot make a device with infinite memory and precision, we utilize converters with limited resolution. There is then a trade-off where higher resolution converters are usually more expensive but offer less distortion than low-resolution converters. In mMIMO systems each RF chain requires both an ADC and a DAC, which results in a significant price increase due to the larger number of converters necessary. In order to reduce costs, we can simply use lower resolution converters that are much cheaper. The downside of these converters is that they introduce more non-linear distortion, [26], as their lower resolution increases the loss of information that occurs in the conversion process.

2.3.4.2 Non-linear Amplification

In a SISO system, the transmitter possesses a single Power Amplifier (PA) that is responsible for amplifying the outgoing signal. In order to not distort the signal this amplifier should be as linear as possible within the signal's dynamic range. The wider the range of symbol energies, the wider the necessary linear operating zone of the amplifier, which in these amplifiers means lower amplification power and, as such, lower energy efficiency, or more expensive amplifiers. We call the process of increasing a PA's linear region at the cost of efficiency *backoff*. For example, a modern 3G BS requires 500W of power to transmit 40W, [27]. This is the main reason for the large energy consumption of the radio access network.

In the case of mMIMO, the sender would require one amplifier per antenna, which for high *backoff* levels would mean a large waste of energy or more expensive devices. It should be noted that the single-carrier system described in the previous section can operate with a low *backoff* due to employing time-domain symbols with equal energy, making the output signal quasi-constant. However, for higher order modulations, like 64-QAM, the signal will exhibit much larger fluctuations and a *backoff* may be required to ensure a linear amplification.

It is therefore important to consider systems with non-linear amplifiers, that is to say, systems with insufficient *backoff*. There is a non-linear distortion introduced when a signal passes through these components.

The signal at the ouput of an ideal PA is the input multiplied by the PA gain, however for large input signals the PA cannot produce the ideal output and instead outputs the maximum power it can deliver. This effect is called "clipping". A model for a commonly used PA, the Solid State Power Amplifier (SSPA), was developed in [28] and characterizes the amplifier's amplitude and phase output for a given amplitude input, also referred as Amplitude-to-Amplitude Modulation (AM/AM) and Amplitude-to-Phase Modulation (AM/PM), respectively. In this model, the AM/AM characteristic has a strictly linear region followed by a transition into a non-linear region, for a linearly increasing input amplitude.

We define the non-linearly amplified signal for a single RF branch at the nth timeslot as

$$A(|s_n|)\exp(j(\arg(s_n)+\Theta(|s_n|))),$$

where $A(\mathbf{s})$ is the AM/AM characteristic and $\Theta(\mathbf{s})$ is the AM/PM characteristic. In the case of an SSPA the AM/PM characteristic is approximately 0, while the AM/AM characteristic is defined as

$$A(|s_n|) = \frac{|s_n|}{\sqrt[2q]{1+\frac{|s_n|^{2q}}{s_M}}}, \tag{2.58}$$

where $|\mathbf{s}|$ is the module of the symbol block, s_M is the clipping level, normalised to the symbol variance, and q is the sharpness of the transition between the linear and the non-linear operating point. For $q=\infty$, a branch function is defined as

$$A(|s_n|) = \begin{cases} |s_n|, & |s_n| \le s_M \\ s_M, & |s_n| > s_M \end{cases}, \tag{2.59}$$

performing as a clipping operation that limits the maximum amplitude of the symbols. The amplified symbol $A(\mathbf{s})$ can also be defined for MIMO systems as $A(\mathbf{s}^{(t)})$ is the tth branch. It can easily be inferred that by maximizing s_M, the distortion can be reduced. However, this severely reduces the power efficiency of SSPAs. In the case of mMIMO where there are several SSPAs, reduced power consumption is a necessity, and with it techniques that reduce these non-linearities.

2.3.5 Security

As with any communication system, there is a need for secure communication. The security is usually implemented under the form of encrypted messages [29] in the upper layers of the Open Systems Interconnection (OSI) model. However, in a wireless system any user can eavesdrop messages being sent in the medium, as depicted in fig. 2.7. If the messages being exchanged could not be understood, it would grant us an additional layer of security, referred to as PLS [30, 31]. A useful metric for the security of a communication is the Secrecy Rate (SCR) [32], which is the difference between the capacity of the system and the capacity of the eavesdropper.

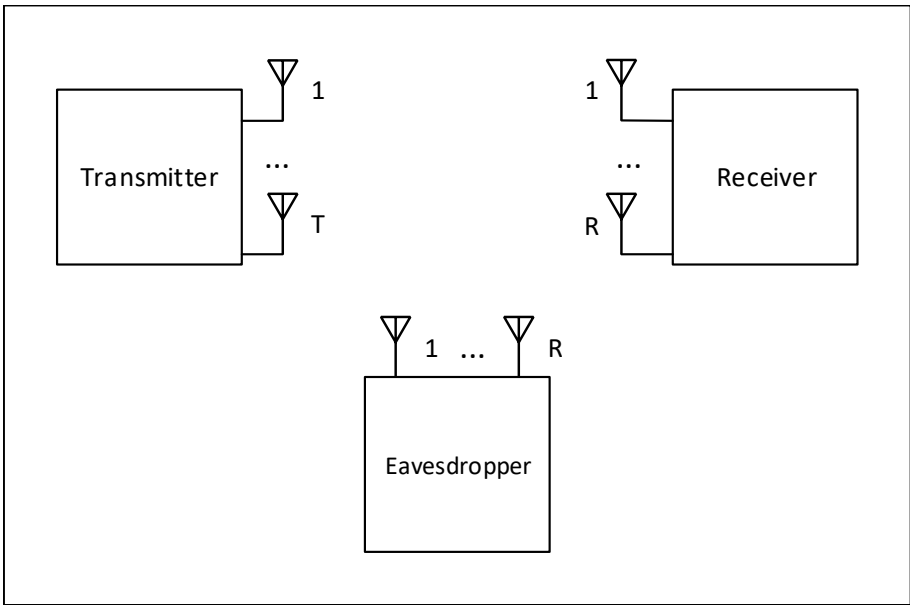

Figure 2.7: Diagram of a MIMO communication between a transmitter and receiver, with an eavesdropper attempting to listen to the conversation.

To calculate the capacities of the systems involved, we use imperfect channel estimates on all users. In the case of the transmitter and intended receiver, the estimates will have a high correlation with the true channel. However, the estimate obtained by the eavesdropper will have a low correlation with the real channel, assuming that the eavesdropper is not within a distance of either user comparable to the wavelength *lambda* in use. We define the channel in this scenario as

$$\mathbf{H}_k = \rho\hat{\mathbf{H}}_k + \epsilon_k, \tag{2.60}$$

where $\hat{\mathbf{H}}_k$ is the channel estimate, ϵ_k is a gaussian distributed error term, and ρ expresses the correlation between the real channel and the channel estimate. In the case of the proper users, this factor will be close to 1, while in the eavesdropper, this factor will in practice be closer to 0. This is assuming that the eavesdropper is not within $\lambda/2$ of either user. Since the channel estimate of the eavesdropper will be much worse, then the

capacity of the eavesdropped system will similarly be lower. This system is, therefore, an interesting solution for physical layer security.

2.4 Proposed Solutions

There is currently a lot of research being done on receivers that can handle the drawbacks of mMIMO, namely in low-complexity receivers that are capable of separating the mMIMO streams, or on cheap receivers that can achieve comparable performances to current receivers while employing highly non-linear elements. The next generation of mobile networks is also expected to offer more robust security options, when compared to the current generation. In that context, we will analyse receivers that address these issues.

We begin by analysing low complexity receivers based on [33] and [34]. These receivers rely on having many antennas at the reception, [35], and we show that coding, [13], can help in reducing the necessary number of antennas. In addition to these schemes, there are alternatives that apply a precoding process at the transmitter, [37], and receivers based on SVD, [36], that split the stream separation process between the transmitter and the receiver. We propose an SVD based receiver that can cope with the differing singular value powers through stream interleaving. This scheme has a high Peak-to-Average Power Ratio (PAPR), so we implement a scheme to estimate and cancel the non-linear distortion based on [38]. Lastly, we examine the peformance of SVD receivers in a security context with an eavesdropper. To this end, we use imperfect channel knowledge to simulate a more practical scenario.

Chapter 3

Efficient Receivers

3.1 Introduction

In this chapter we will introduce techniques that improve receiver efficiency. First, we look at low-complexity techniques and how to improve their performance. These techniques generally have lower performance compared to traditional schemes, but are much more efficient in computation time. We will show that the drawbacks of these techniques can be partly mitigated with the use of error correcting codes.

Secondly, we will analyse a receiver that is much more complex than the first receivers, but can be improved with non-linear distortion cancelling techniques. As we will see, this receiver is much more efficient in terms of energy consumption. In addition, we combine this receiver with an error correction code, in order to improve the distortion cancelling.

3.2 Low Complexity Receivers

Although mMIMO can offer significantly higher data rates, the complexity added can increase overall system delay. In order to obtain the capacity described in 2.51, a high performance equalization process is required, such as MMSE. However, this type of equalization relies on computing inverse channel matrices of dimension T by R, which in the case of mMIMO, with very large values of T and R, can introduce a large delay in the system. As such, there is a need for simpler equalization schemes, such as Maximum-Ratio Combining (MRC) and Equal-Gain Combining (EGC) based receivers.

These schemes, as described in [35], operate on the principle that for $R >> 1$ and small correlation between different transmit and receive antennas, we can simplify our channel matrix into a quasi diagonal matrix. Computing the inverse of a diagonal matrix is simply multiplying by another diagonal matrix where each value is the inverse of the original

matrix, a far simpler process than computing regular inverse matrices.

The disadvantage of these receivers is that to meet the required performance very large values of R are needed, which may not be feasible in practice. As such, techniques to boost performance of these receivers are being studied. One such technique is employing iterative receivers based on IB-DFE in order to reduce ISI, described in [33] and [34]. Since the equalization process is far simpler than MMSE, the extra complexity introduced by a few iterations is fairly insignificant.

3.2.1 Maximal-Ratio Combiner

This type of technique is usually employed in systems with more receive antennas than transmit antennas, as described in [39]. A receiver with this configuration receives multiple samples of the same signal which can then be combined into an averaged signal.

This receiver operates on the assumption that the channels between the receiver and sender are independent, that is, have low correlation, which allows the approximation

$$\mathbf{H}_k^H \mathbf{H}_k \approx R\mathbf{I}. \tag{3.1}$$

This approximation greatly simplifies the equalization process defined in 2.17 and (2.19) by defining

$$\mathbf{A}_k = \mathbf{H}_k^H. \tag{3.2}$$

Since the IB-DFE described in (2.2.3) assumes the arriving signal power to have unitary average, then a normalization factor must be defined. The normalization factor $\mathbf{\Psi}$ can be computed as a diagonal matrix where each element (t,t) is defined as

$$\mathbf{\Psi}^{(t,t)} = (\sum_{k=0}^{N-1} \sum_{r=1}^{R} |H_k^{(r,t)}|^2)^{-1}. \tag{3.3}$$

This factor is combined with 3.2 and rewrites it as

$$\mathbf{F}_k = \mathbf{\Psi}\mathbf{H}_k^H. \tag{3.4}$$

We can improve this receiver's performance by employing the IB-DFE technique, with the above $\mathbf{F}_k$ factor definition. The MRC can be employed in an iterative fashion as in the conventional IB-DFE with MMSE, leading to a receiver known as Maximal-Ratio Detector (MRD).

To measure the performance of this receiver, we considered, Monte Carlo simulations of a fading Rayleigh channel with $I = 16$ uncorrelated rays, and 1000 blocks of size of $N = 256$. In fig. 3.1, we observe that, without iterations, the MRD requires very large receiving antenna arrays in order to improve performance. However, the introduction of the iterative receiver greatly reduces the necessary number of receiving antennas.

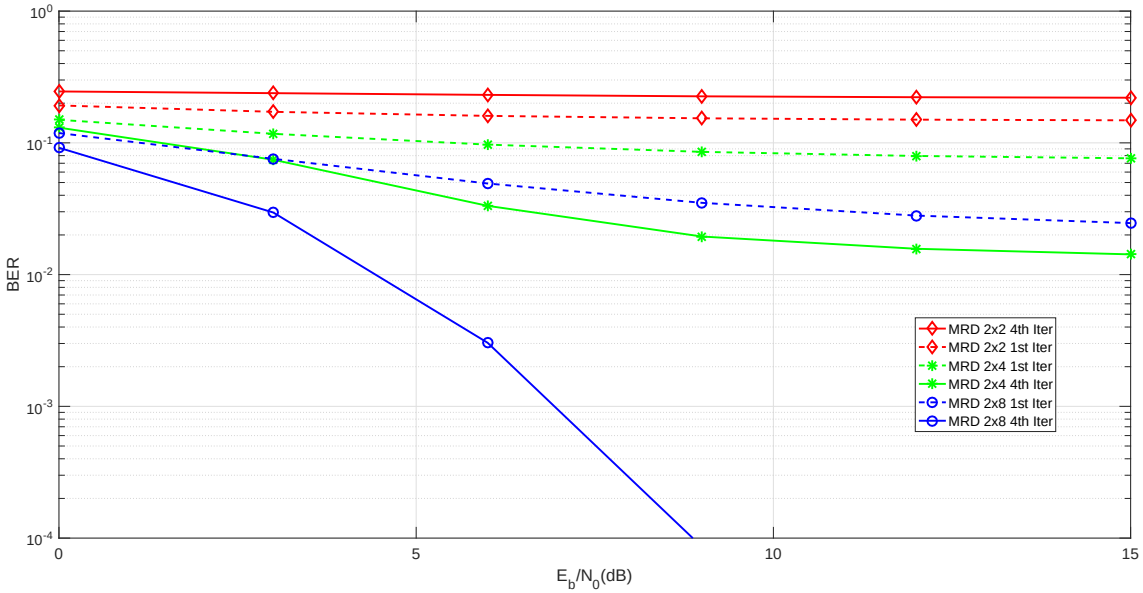

Figure 3.1: BER for different MIMO-MRD configurations, employing QPSK. Results are shown for the first and fourth iterations of the iterative receiver.

3.2.2 Equal-Gain Combiner

Another receiver technique is the EGC, which is based on the same principle as the MRC technique of having more receiving antennas than transmitting antennas. In such a scenario, and assuming that there is low correlation between the different receiving and transmitting channels, the it is possible to approximate

$$\mathbf{A}_k^H \mathbf{H}_k, \tag{3.5}$$

as a diagonal matrix. This matrix $\mathbf{A}_k$ is defined as

$$\mathbf{A}_k = \exp(j \arg(\mathbf{H}_k)). \tag{3.6}$$

This approximation can then be applied to (2.17) and (2.19) by defining $\mathbf{F}_k$ as

$$\mathbf{F}_k = \mathbf{\Psi} \mathbf{A}_k^H, \tag{3.7}$$

with $\mathbf{\Psi}$ being a normalization factor equal to the one defined in (3.3) for the MRC technique. Similar to the MRD, we apply the IB-DFE to this receiver, using the $\mathbf{F}_k$ definition in (3.7), in order to decrease the necessary number of receive antennas. This iterative receiver is referred to as Equal-Gain Detector (EGD).

We measure the performance of this receiver with the same conditions as the MRD, using 1000 blocks of 256 symbols. From fig. 3.2 we observe that, without iterations, this receiver requires very large numbers of receiving antennas to obtain acceptable performances. However, performing the iterations provides a significant boost to performance, thereby reducing the necessary number of antennas. In comparison with the MRD, the EGD can achieve better performance for lower ratios of R/T, however for higher ratios the MRD should be considered.

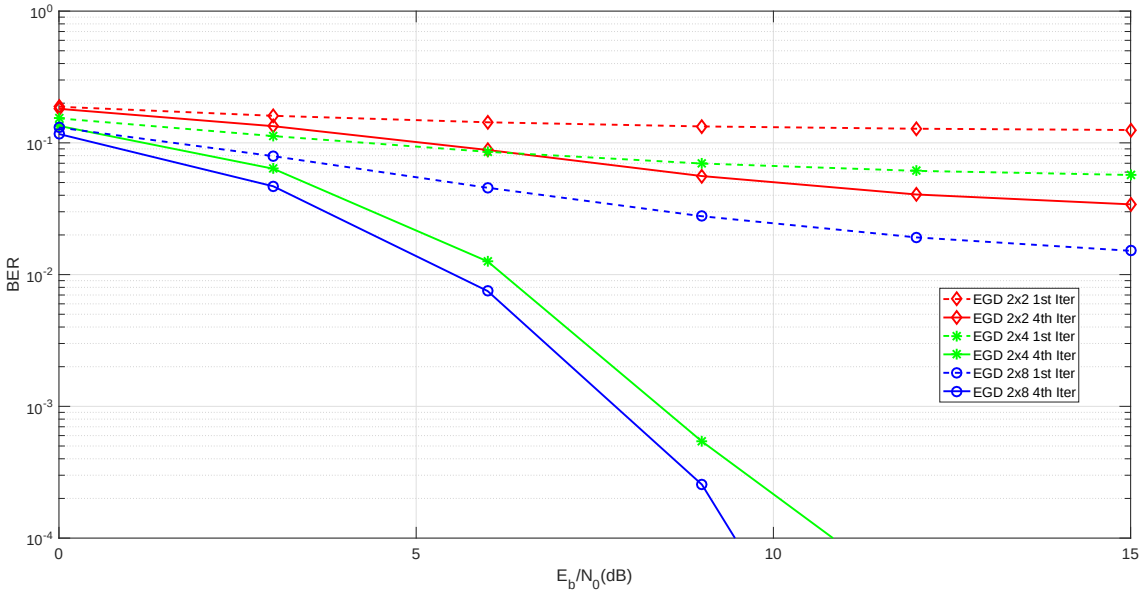

Figure 3.2: BER for different MIMO-EGD configurations, with QPSK. Results are shown for the first and fourth iterations of the iterative receiver.

3.3 APP Decoding

In order to further reduce the necessary number of receive antennas, we study the performance of the EGD and MRD combined with a 64-state convolutional code with APP decoding. We obtained the BER for these receivers through simulations as before, but with a larger block count of 10000. We focus our analysis on the performance of the last iterations, as each iteration of these receivers is of low computational complexity.

In Fig. 3.3, we observe that the EGD can achieve significantly better performance for lower ratios of R/T, with only a 6 dB difference between the fourth iteration with ratios of 1 and 4, and less than 1 dB between the ratios 2 and 4. Fig. 3.4 shows the BER of the coded MRD, where we observe that when $R/T = 1$, the BER has improved. However, the significant improvement comes in the fourth iteration with $R/T = 2$ and $R/T = 4$. The difference between these two MIMO configurations is about 1 dB. A stark contrast with the uncoded MRD that achieved a much larger difference. In order to outperform the EGD for the same ratio R/T, the MRD required $R/T = 4$, while with convolutional coding, the MRD achieves a similar performance to the EGD with $R/T = 2$, in the fourth iteration.

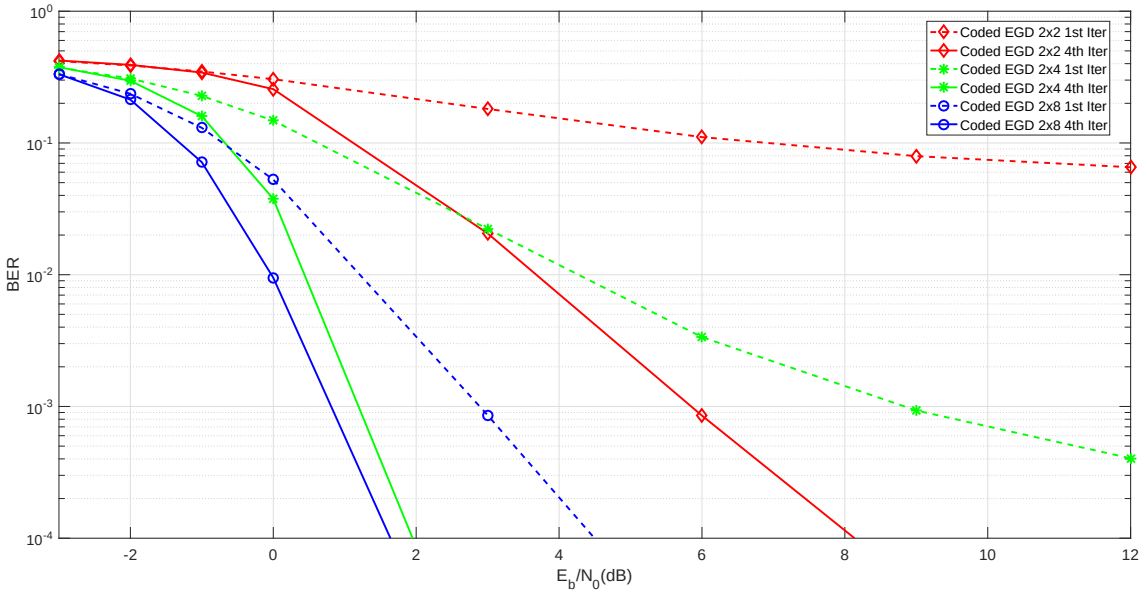

Figure 3.3: BER for various MIMO configurations, with QPSK and a 64 state convolutional code. Results are shown for the first and fourth iterations of the iterative receiver.

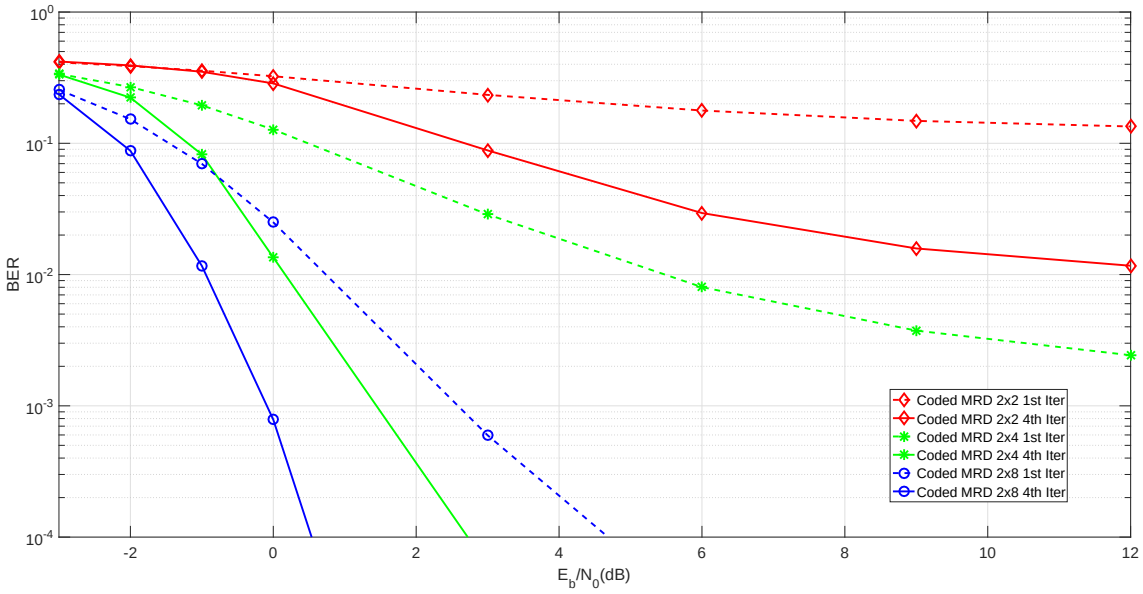

Figure 3.4: BER for various MIMO configurations, with QPSK and a 64 state convolutional code. Results are shown for the first and fourth iterations of the iterative receiver.

3.4 Singular Value Decomposition

We have seen equalization methods with little complexity that suffer from high interference caused by neighbouring channels in mMIMO systems. Now we shall present a technique that greatly reduces this interference, at the cost of higher complexity at the transmitter and receiver.

An attractive technique that combines precoding at the transmitter and decoding at the receiver is an SVD based technique [36]. Using this technique, we can decompose the channel matrix $\mathbf{H}_k$, defined in (2.55), as

$$\mathbf{H}_k = \mathbf{U}_k \mathbf{\Lambda}_k \mathbf{V}_k^H, \tag{3.8}$$

where $\mathbf{U}_k$ is the $R \times R$ decoding matrix, $\mathbf{V}_k$ is the $T \times R$ precoding matrix and $\mathbf{\Lambda}_k$ is the $R \times R$ singular values matrix. Using this decomposition, we define two operations, one in the transmitter and one in the receiver.

3.4.1 Transmitter

The transmitter is the same as previously defined in Chapter 2, employing M-QAM. Using the symbols $\mathbf{S}_k$, defined as the frequency counterpart of (2.54), we define the precoding operation as

$$\mathbf{X}_k = \mathbf{V}_k \mathbf{S}_k. \tag{3.9}$$

The $T \times 1$ vector $\mathbf{X}_k$ represents the precoded signal that will be transmitted.

3.4.2 Receiver

The received signal is defined as

$$\mathbf{Z}_k = \mathbf{H}_k \mathbf{X}_k + \mathbf{N}_k. \tag{3.10}$$

In order to complete the SVD technique, the receiver computes the decoding process as

$$\mathbf{W}_k = \mathbf{U}_k^H \mathbf{Z}_k. \tag{3.11}$$

We can expand these equations, in order to define the resulting signal from this technique as

$$\begin{aligned} \mathbf{W}_k &= \mathbf{U}_k^H \mathbf{H}_k \mathbf{X}_k + \mathbf{U}_k^H \mathbf{N}_k \\ &= \mathbf{U}_k^H \mathbf{H}_k \mathbf{V}_k \mathbf{S}_k + \mathbf{U}_k^H \mathbf{N}_k \\ &= \mathbf{U}_k^H \mathbf{U}_k \mathbf{\Lambda}_k \mathbf{V}_k^H \mathbf{V}_k S_k + \mathbf{U}_k^H \mathbf{N}_k \\ &= \mathbf{\Lambda}_k \mathbf{S}_k + \mathbf{U}_k^H \mathbf{N}_k. \end{aligned} \tag{3.12}$$

Since $\mathbf{\Lambda}_k$ is a diagonal matrix, separating the different streams is now simply dividing by the corresponding singular values. In addition, as $\mathbf{U}_k$ is a unitary matrix, the noise power remains the same. It should be noted that we are assuming that all singular values exist,

that is, that the different channels are uncorrelated. By assuming that the antennas are reasonably spaced between themselves, then it becomes safe to assume that the channels have low correlation.

Lastly, we perform an equalization based on the MMSE criterion, defined as

$$\tilde{\mathbf{S}}_k = \frac{\mathbf{W}_k \mathbf{\Lambda}_k}{\mathbf{\Lambda}_k^2 + \frac{1}{\mathrm{SNR}}}, \tag{3.13}$$

where $\tilde{\mathbf{S}}_k$ are the corresponding symbol estimations. We can use this definition due to the fact that we assume that all singular values exist, which makes Λ_k a real diagonal matrix, with an inverse matrix that always exists and is, likewise, also a diagonal matrix.

Although this technique correctly separates each stream, not all singular values will have the same power. Fig. 3.5 shows the singular values distribution for an 8×8 system, obtained from 100 channel realizations. From the figure, it can be observed that there is a significant power difference between the singular values. The streams affected by the lower power singular values will have a much worse performance, bringing down the average throughput of this receiver. In addition, since each stream is affected by singular values that follow the same distribution, the channel can be viewed as flat for that stream, making techniques such as IB-DFE ineffective. A common solution is to implement power compensation on the streams with lower singular values, as seen in [40]. Alternatively, we propose a simple interleaving scheme between the different streams, that can improve the average performance of all streams by forcing them to have equal average power, and make the equivalent channel be frequency-selective, to allow for the use of the IB-DFE technique.

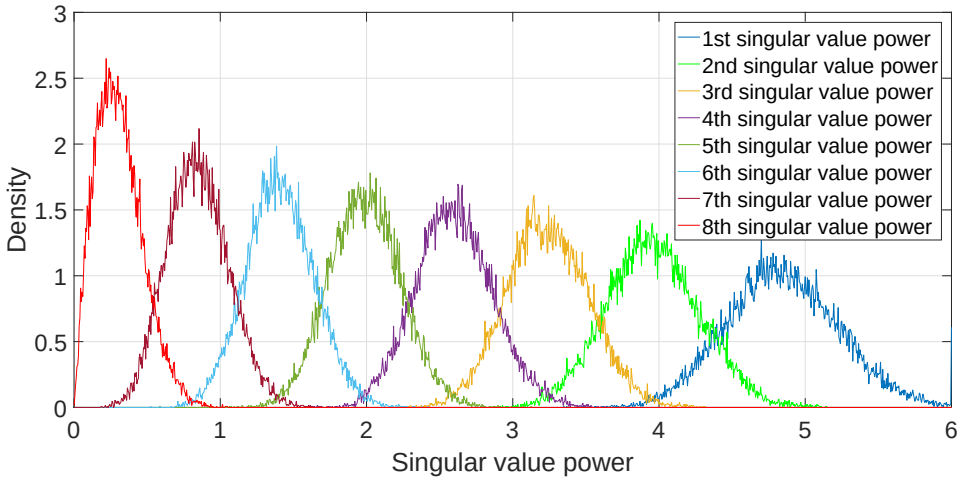

Figure 3.5: Probability Density Function (PDF) of the singular values in an 8×8 system.

3.4.3 Interlevead MIMO-SVD for SC-FDE

The interleaving mixes all streams in equal proportion, in order to have all values affect each stream equally, and is performed in the frequency-domain, as shown in Fig. 3.6. This

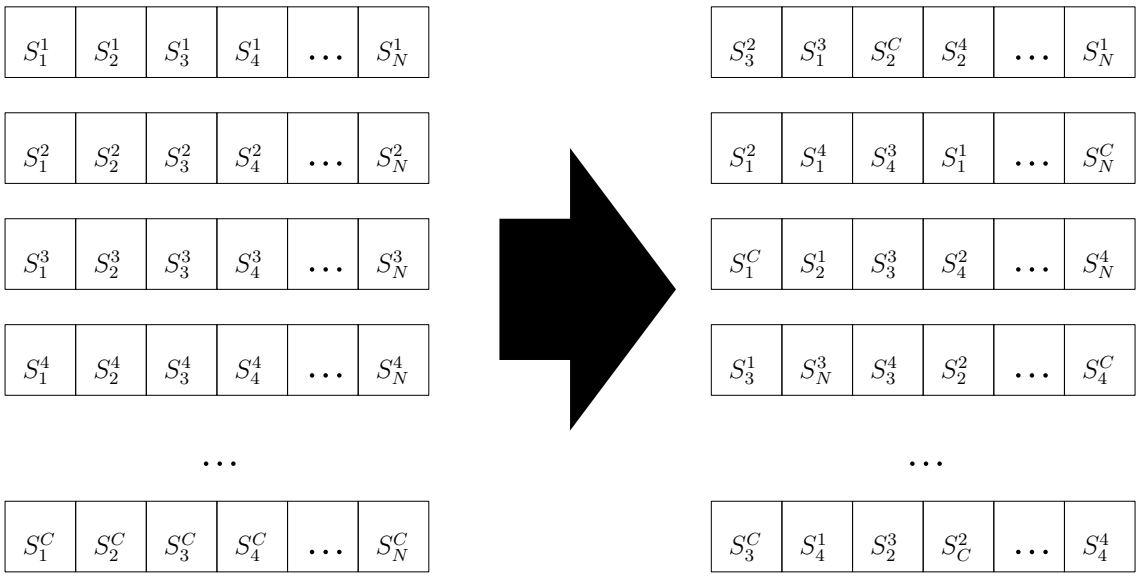

Figure 3.6: Diagram of the interleaving applied to the frequency-domain symbols.

technique requires that the block size N be larger than the number of singular values, which will be the case of most systems. The transmitter applies this interleaving to the symbols, $\mathbf{S}_k$, before the precoding operation. We define the interleaved vector as $\mathbf{S}'_k$. We now redefine (3.9) as

$$\mathbf{X}'_k = \mathbf{V}_k \mathbf{S}'_k. \tag{3.14}$$

The received signal can be rewritten as

$$\mathbf{Z}'_k = \mathbf{H}_k \mathbf{X}'_k + \mathbf{N}_k. \tag{3.15}$$

In the receiver side, the decoding process is, similarly, rewritten as

$$\mathbf{W}'_k = \mathbf{U}_k^H \mathbf{Z}'_k, \tag{3.16}$$

and expanded as

$$\begin{aligned} \mathbf{W}'_k &= \mathbf{U}_k^H \mathbf{H}_k \mathbf{X}'_k + \mathbf{U}_k^H \mathbf{N}_k \\ &= \mathbf{U}_k^H \mathbf{H}_k \mathbf{V}_k \mathbf{S}'_k + \mathbf{U}_k^H \mathbf{N}_k \\ &= \mathbf{U}_k^H \mathbf{U}_k \mathbf{\Lambda}_k \mathbf{V}_k^H \mathbf{V}_k S'_k + \mathbf{U}_k^H \mathbf{N}_k \\ &= \mathbf{\Lambda}_k \mathbf{S}'_k + \mathbf{U}_k^H \mathbf{N}_k. \end{aligned} \tag{3.17}$$

With the SVD technique complete, the receiver must now restore the original symbol order between the streams. Applying the deinterleaving technique, obtaining

$$\mathbf{W}_k = \mathbf{\Lambda}'_k \mathbf{S}_k + \mathbf{U}_k^{'H} \mathbf{N}'_k, \tag{3.18}$$

where $\mathbf{\Lambda}'_k$ is the singular values matrix after applying the deinterleaving, which will be used in the equalization process.

Since the equivalent channel for each stream is now composed of all singular values, it can be viewed as an equivalent frequency-selective channel. As such, we employ the receiver introduced in the subsection 2.2.3 as

$$\tilde{\mathbf{S}}_k^{(i)} = \mathbf{F}_k^{(i)}\mathbf{W}_k - \mathbf{B}_k^{(i)}\bar{\mathbf{S}}_k^{(i-1)}, \tag{3.19}$$

where i corresponds to the ith equalization iteration of this receiver. We must also redefine the feedforward and feedback factors, $\mathbf{F}_k$ and $\mathbf{B}_k$, respectively.The feedback matrix $\mathbf{F}_k$ is defined as

$$\mathbf{F}_k^{(i)} = \frac{\mathbf{\Lambda'}_k}{\left(1 - \left|\rho^{(i-1)}\right|^2\right)\mathbf{\Lambda'}_k^2 + \frac{1}{\mathrm{SNR}}}, \tag{3.20}$$

and $\mathbf{B}_k$ as

$$\mathbf{B}_k^{(i)} = \mathbf{F}_k^{(i)}\mathbf{\Lambda}'_k - \mathbf{I}. \tag{3.21}$$

The soft decision calculation is not affected by the interleaving and is performed as described in subsection 2.2.4.

3.4.4 Performance

This subsection presents a set of performance results regarding the proposed interleaved SVD scheme. In all simulations 1000 blocks of size $N = 512$ were transmitted over a channel with a Rayleigh distribution, and $I = 16$ uncorrelated rays is considered. From Fig. 3.7, it can be observed that the receiver can reach an adequate performance, thanks to the gain associated with performing several equalization iterations. As in the case of IB-DFE, there is a performance degradation when higher order modulations are employed. Although this receiver does not outperform the IB-DFE, it does offer two advantages. First is the reduced complexity of each individual iteration, although this may be offset by the computation power necessary to compute the SVD matrices. Secondly, and more importantly, this system does not directly transmit data symbols, but instead transmits the precoded data symbols, which approximately have a Gaussian distribution. This allows us to employ a non-linear distortion cancelling technique that will be detailed in the following section.

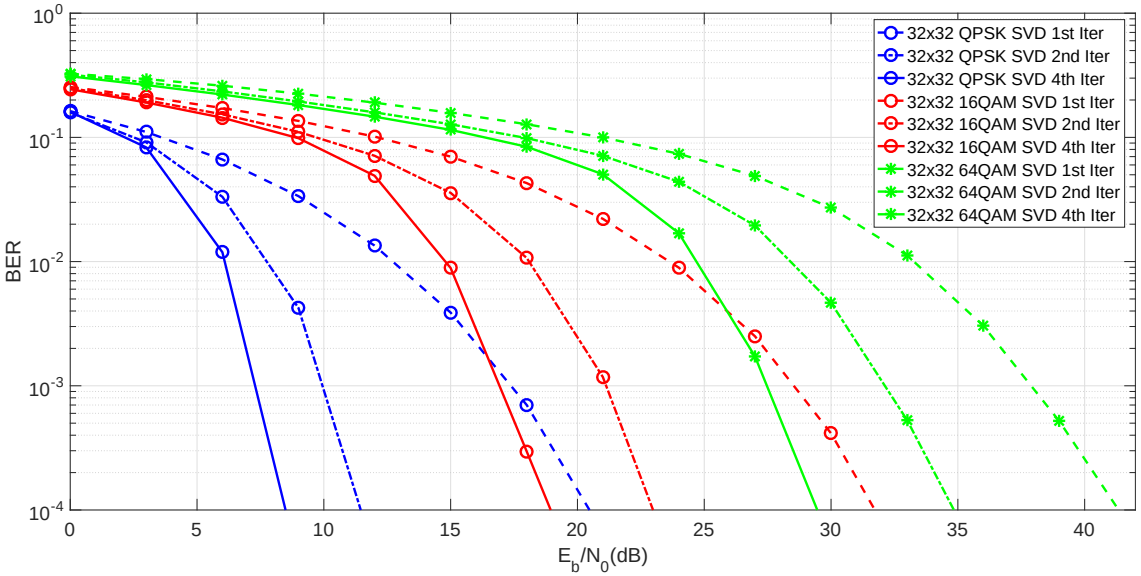

Figure 3.7: Comparison of the BER for $R = T = 32$ MIMO SVD system for different QAM constellations.

3.5 Bussgang Receiver

Let us now consider the same SVD based system, now with the non-ideal SSPAs described in subsection 2.3.4.2, as shown in Fig. 3.8. This amplifier has a negligible AM/PM characteristic, while its AM/AM characteristic is defined, for a single branch at the nth timeslot, as

$$A(|x_n|) = \frac{|x_n|}{\sqrt[2q]{1 + \frac{|x_n|^{2q}}{s_M}}}, \tag{3.22}$$

and our transmitted signal is defined as

$$y_n = A(|x_n|)\exp(j(arg(x_n))). \tag{3.23}$$

As can be observed from Fig. 3.9, the precoded signal presents a large PAPR, which means that the transmitted signal might suffer from severe nonlinear distortion effects, leading to performance degradation. Although the typical advantage attributed to SC systems are the low envelope fluctuations, which permits the use of highly nonlinear amplifiers, this is only the case for QPSK systems. For M-QAM systems, the envelope of an SC signal can have large fluctuations, that substantially increase with M. Therefore, the addition of the precoding technique, that might further increase the PAPR, does not conflict with the advantages of SC-FDE systems, and can even be beneficial in this scenario.

The precoded signal, $\mathbf{X}_k$, follows a Gaussian distribution, as described in [41] and shown in Fig. 3.10, which allows us to employ a non-linear distortion cancelling technique based on the Bussgang Theorem [38]. By taking advantage of this theorem, we can decompose the distorted signal as the sum of two uncorrelated terms: a term that is equal to the original signal scaled down by a constant; and a noisy term associated to the

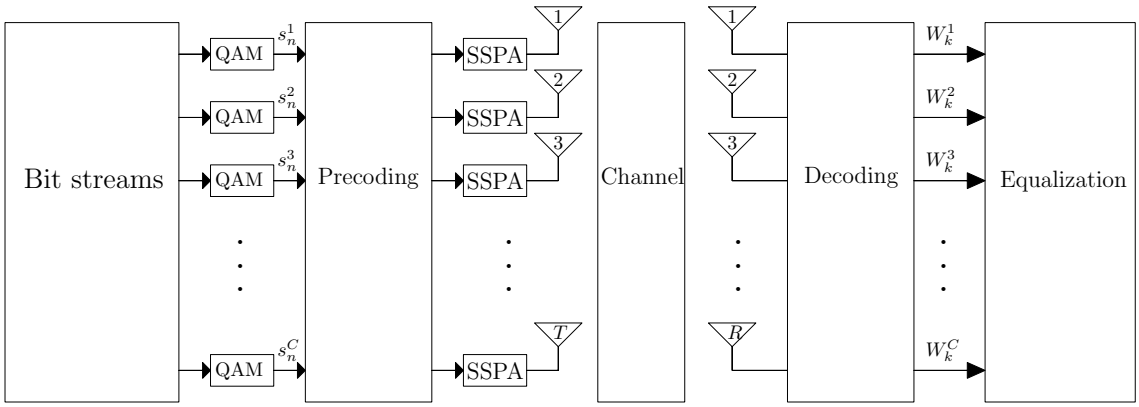

Figure 3.8: Diagram of our SVD based system with non-ideal amplification.

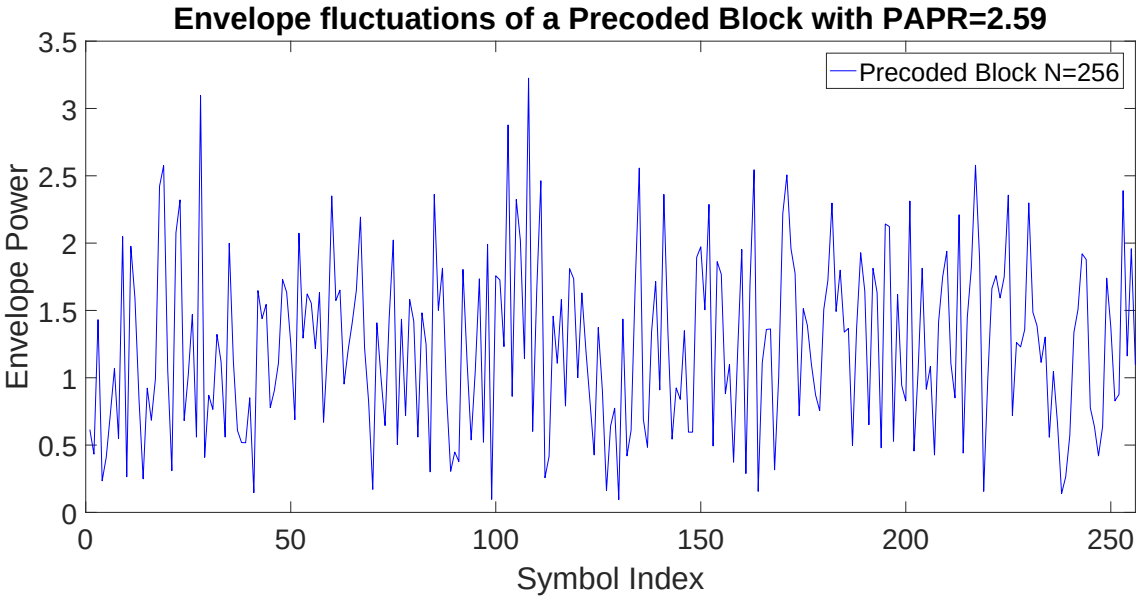

Figure 3.9: PAPR of a single block with 256 QPSK symbols.

non-linear distortion. Let us define the amplified signal for the tth branch at the nth time instant as

$$y_n^{(t)} = \alpha^{(t)} x_n^{(t)} + d_n^{(t)}, \tag{3.24}$$

with $\alpha^{(t)}$ being the scale factor applied to the original signal and $d_n^{(t)}$ our distortion term. The scale factor $\alpha^{(t)}$ is calculated by

$$\alpha^{(t)} = \frac{\mathbb{E}\left[x_n^{(t)} y_n^{*(t)} \exp(-j\Theta(|x_n^{(t)}|))\right]}{\mathbb{E}\left[\left|x_n^{(t)}\right|^2\right]}, \tag{3.25}$$

which in the case of the SSPA becomes

$$\frac{\mathbb{E}\left[x_n^{(t)} y_n^{*(t)}\right]}{2\sigma_x^2} \tag{3.26}$$

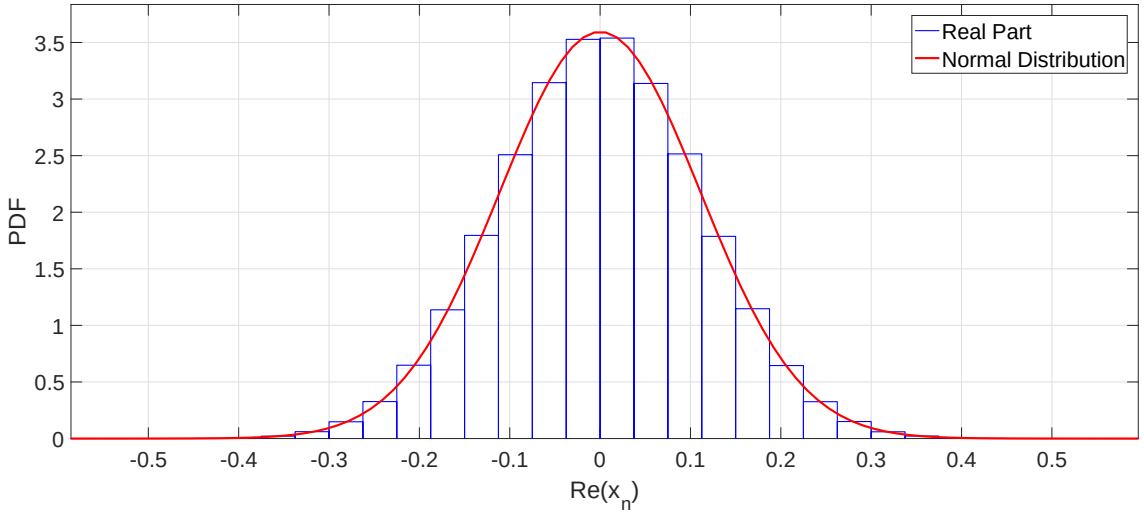

Figure 3.10: Distribution of the real part of the outgoing signal before amplification.

If we assume that the amplifiers for each transmit branch are all the same, then the scale factor α is the same for all streams. The same decomposition can be performed in the frequency domain, netting the frequency domain symbols and distortion as

$$Y_k^{(t)} = \alpha \mathbf{X}^{(t)} + \mathbf{D}^{(t)}, \tag{3.27}$$

where $\mathbf{D}^{(t)}$ is the frequency-domain version of the distortion term along the tth branch. To simplify the analysis we will focus on the symbols at the kth subcarrier,

$$Y_k^{(t)} = \alpha \mathbf{X}_k + \mathbf{D}_k. \tag{3.28}$$

Under these conditions we can decompose the received nonlinearly-distorted signal as

$$\mathbf{Z}_k' = \mathbf{H}_k(\alpha \mathbf{X}_k' + \mathbf{D}_k)) + \mathbf{N}_k. \tag{3.29}$$

Our decoded signal can, likewise, be rewritten as

$$\begin{aligned} \mathbf{W}_k' &= \mathbf{U}_k^H \mathbf{H}_k(\alpha \mathbf{X}_k' + \mathbf{D}_k) + \mathbf{U}_k^H \mathbf{N}_k \\ &= \mathbf{U}_k^H \mathbf{H}_k(\alpha \mathbf{V}_k \mathbf{S}_k' + \mathbf{D}_k) + \mathbf{U}_k^H \mathbf{N}_k \\ &= \mathbf{U}_k^H \mathbf{U}_k \mathbf{\Lambda}_k \mathbf{V}_k^H(\alpha \mathbf{V}_k S_k' + \mathbf{D}_k) + \mathbf{U}_k^H \mathbf{N}_k \\ &= \mathbf{\Lambda}_k \alpha \mathbf{S}_k' + \mathbf{U}_k^H \mathbf{H}_k \mathbf{D}_k + \mathbf{U}_k^H \mathbf{N}_k, \end{aligned} \tag{3.30}$$

with the deinterleaved symbols given by

$$\mathbf{W}_k = \mathbf{\Lambda}_k \alpha' \mathbf{S}_k + \mathbf{U}_k^{'H} \mathbf{H}_k' \mathbf{D}_k' + \mathbf{U}_k^{'H} \mathbf{N}_k'. \tag{3.31}$$

From (3.31) it can be shown that the received symbols are scaled by α_n, and the signal has increased distortion due to the $\mathbf{U}_k^{'H} \mathbf{H}_k' \mathbf{D}_k'$ factor. The main objective of our receiver is to equalize the signal based on the reduced symbol power and distortion power, as well as attempt to estimate and cancel the interference term, so as to reduce the degradation due to the distortion.

In order to take into account the distorted signal power, let us rewrite (3.20) as

$$\mathbf{F}_k^{(i)} = \frac{\mathbf{\Lambda'}_k}{\left(1 - \left|\rho^{(i-1)}\right|^2\right)\mathbf{\Lambda'}_k^2 + \frac{1}{\alpha^2 \text{SNDR}}}, \tag{3.32}$$

where SNDR is our Signal-to-Noise plus Distortion Ratio (SNDR) that is simply

$$SNDR = \frac{P_s}{P_N + P_D}, \tag{3.33}$$

where P_s is the signal power, P_N is the noise power and P_D is the power associated to the distortion term. By taking into account the power degradation due to the non-linearity, we can improve performance for higher SNRs. The same reasoning is applied to the calculation of the soft decisions, as we can redefine (2.23) as

$$\sigma_i^2 = P_N + P_D. \tag{3.34}$$

We can compute the distortion term's power by resorting to the truncated Inter-Modulation Product (IMP) approach, shown in [42], to compute the higher order IMPs. However, in order to maintain simplicity, we will compute the distortion power through simulations.

To mitigate the performance degradation associated to the nonlinear distortion, we can also attempt to cancel the noisy distortion term $\mathbf{U}_k^{'H}\mathbf{H}_k'\mathbf{D}_k'$. After the first iteration of our receiver, having obtained the first symbol estimate, $\hat{\mathbf{s}}_n$, we can calculate the distortion term by computing

$$\hat{\mathbf{d}}_n^{(i)} = A(\hat{\mathbf{x}}_n) - \alpha\hat{\mathbf{x}}_n, \tag{3.35}$$

where $\hat{\mathbf{x}}_n$ is the time-domain version of $\mathbf{V}_k\hat{\mathbf{S}}_k$, and $\hat{\mathbf{D}}_k^{(i)}$ is the frequency domain of the distortion term estimate $\hat{\mathbf{d}}_n^{(i)}$. The next step is to reproduce the transmission chain using the distortion term estimate, in order to obtain the term $\mathbf{U}_k^{'H}\mathbf{H}_k'\hat{\mathbf{D}}_k^{'(i)}$. With the distortion estimate calculated, we can rewrite (3.19) in order to cancel the distortion term as

$$\tilde{\mathbf{S}}_k^{(i)} = \mathbf{F}_k^{(i)}(\mathbf{W}_k - \mathbf{U}_k^{'H}\mathbf{H}_k'\hat{\mathbf{D}}_k^{'(i-1)}) - \mathbf{B}_k^{(i)}\bar{\mathbf{S}}_k^{(i-1)}, \tag{3.36}$$

with $\hat{\mathbf{D}}_k^{'(0)} = 0$. The block diagram of the proposed receiver is shown in Fig. 3.11.

3.5.1 Performance

Let us now observe the non-linearity distortion cancelling effect on the performance of the receiver. The following results were obtained through Monte Carlo simulations for 1000 blocks of 512 symbols each, sent through a fading channel with 16 uncorrelated Rayleigh distributed rays.

Fig. 3.12 presents the impact of the non-linearity in a 16-QAM system with $R = T = 32$. When $s_M/\sigma_x = 4$, we have a degradation of about 7 dB for a target BER of 10^{-4}, while the gain from the IB-DFE iterations is the same even with the added distortion. However,

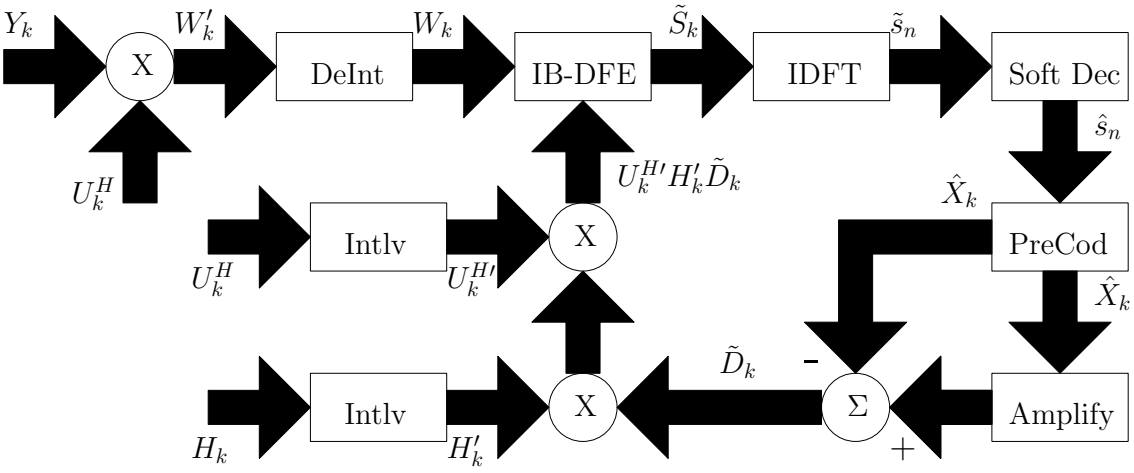

Figure 3.11: Diagram of the proposed SVD receiver.

for $s_M/\sigma_x = 2$, the receiver's performance is significantly worse, and the BER floor is substantially higher in this case.

As can be observed in Fig. 3.13, the addition of the Bussgang cancelling provides a much needed boost in performance for systems with this type of distortion. Although the first iteration may not improve, or even be worse in this scenario, the iterative gain of the distorted system is much higher due to the distortion cancelling. By comparing with the linear receiver, we have a gain of 6 dB when the BER is 10^{-4} and the clipping level is $s_M/\sigma_x = 4$, and a lowered BER floor for a clipping level of 2.

For an increased modulation order of 64-QAM we have in Fig. 3.14 the BER of the linear receiver, and in Fig. 3.15 the Bussgang receiver. Due to the larger constellation, the symbols require more linear amplification. This reflects in a severe performance degradation even for higher clipping levels than the 16-QAM receiver. As such, the increase in performance of the Bussgang receiver is much larger. Particularly, for $s_M/\sigma_x = 4$, the receiver achieves only a 6 dB degradation over the non-distorted ideal receiver.

3.5.2 Coded Bussgang Receiver

The performance of the Bussgang receiver depends heavily on the quality of the equalized symbols. We can improve that quality by employing the error correcting code introduced in Sec. 3.3. However, this decoder does not take into account the non-linear distortion present in the coded bits. As such, we can improve the performance of the coded system further by taking into account the distortion noise power.

The APP decoder's input is bit LLRs, which are computed based on the symbol variance of the received block. In the linear receiver, the LLR inputs to the decoder are calculated using (2.23), which does not take into account the effect of the nonlinear distortion. This fact can limit the performance of the decoder. By using the definition in (3.34), we can achieve a significantly better performance even on the first iteration.

We now simulate the coded receivers under the same conditions as before, with lower

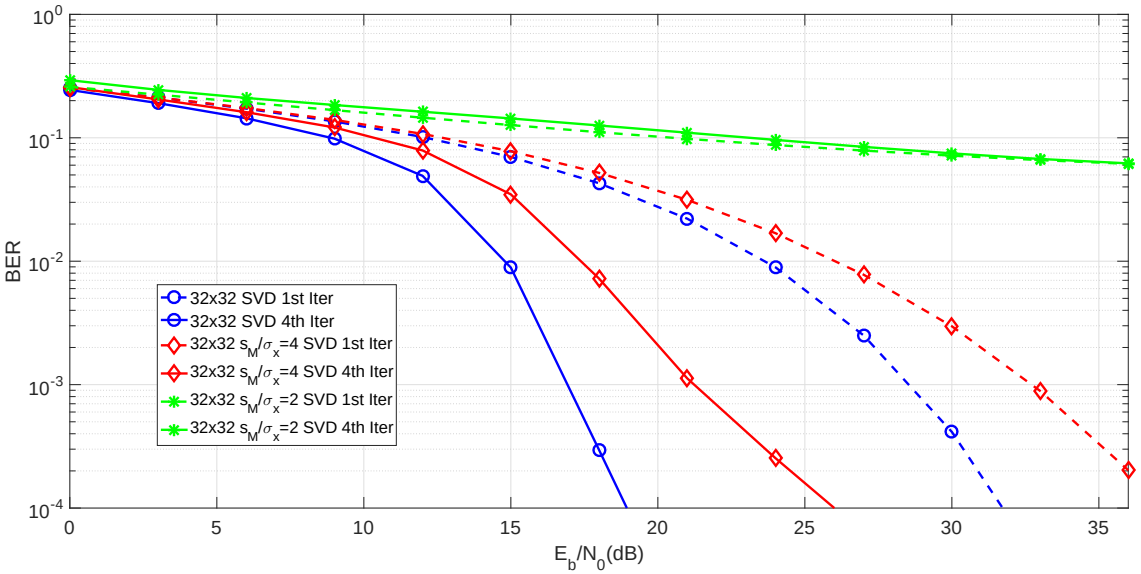

Figure 3.12: BER for a $R = T = 32$ MIMO SVD system employing 16-QAM, with various clipping levels.

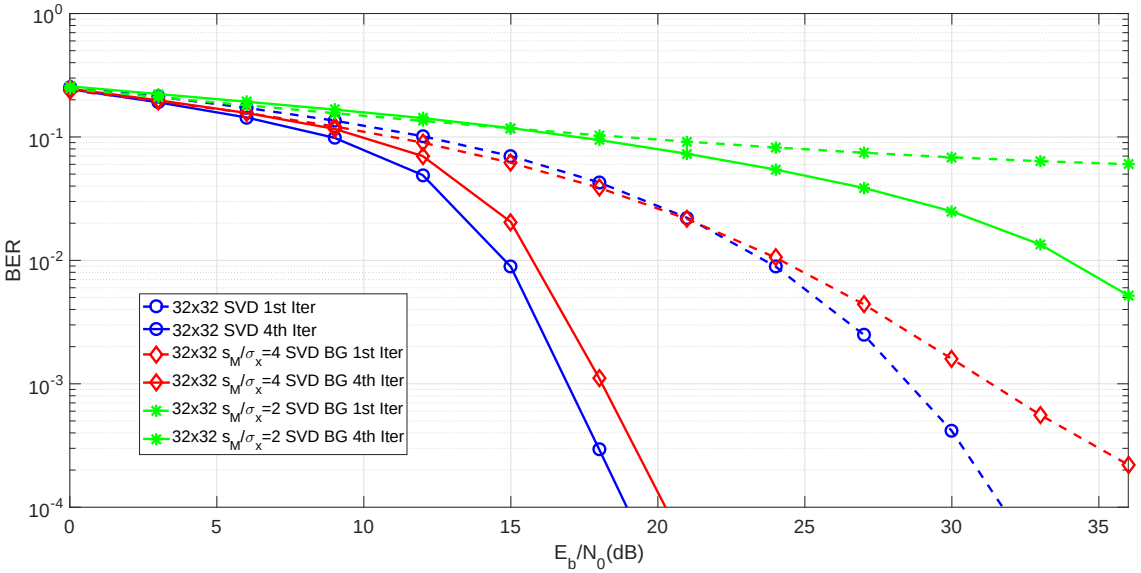

Figure 3.13: BER for a $R = T = 32$ MIMO SVD system with Bussgang cancelling, employing 16-QAM, for various clipping levels.

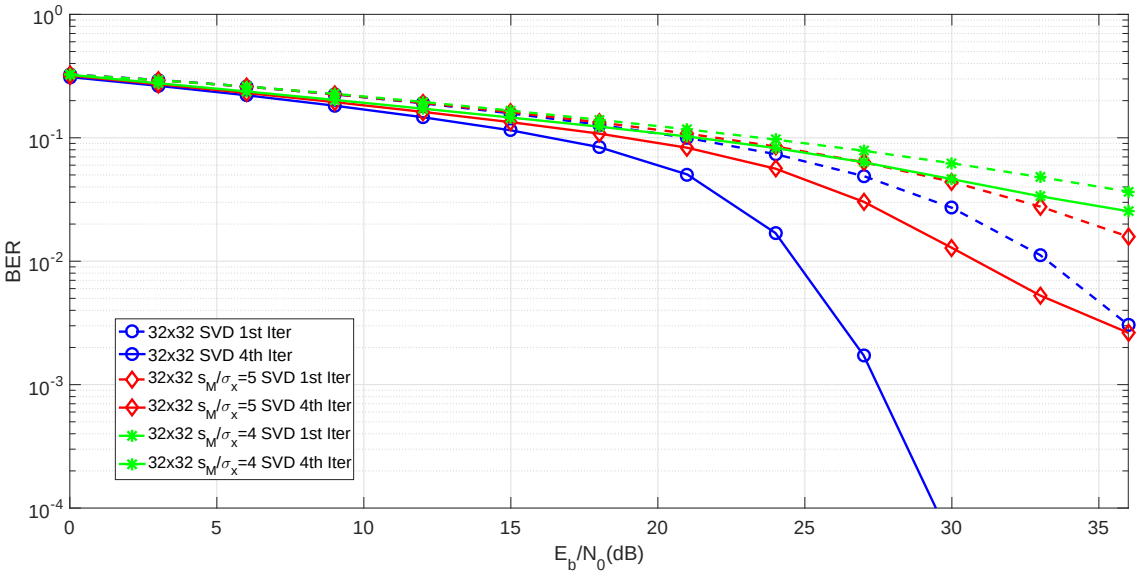

Figure 3.14: BER for a $R = T = 32$ MIMO SVD system employing 64-QAM, with various clipping levels.

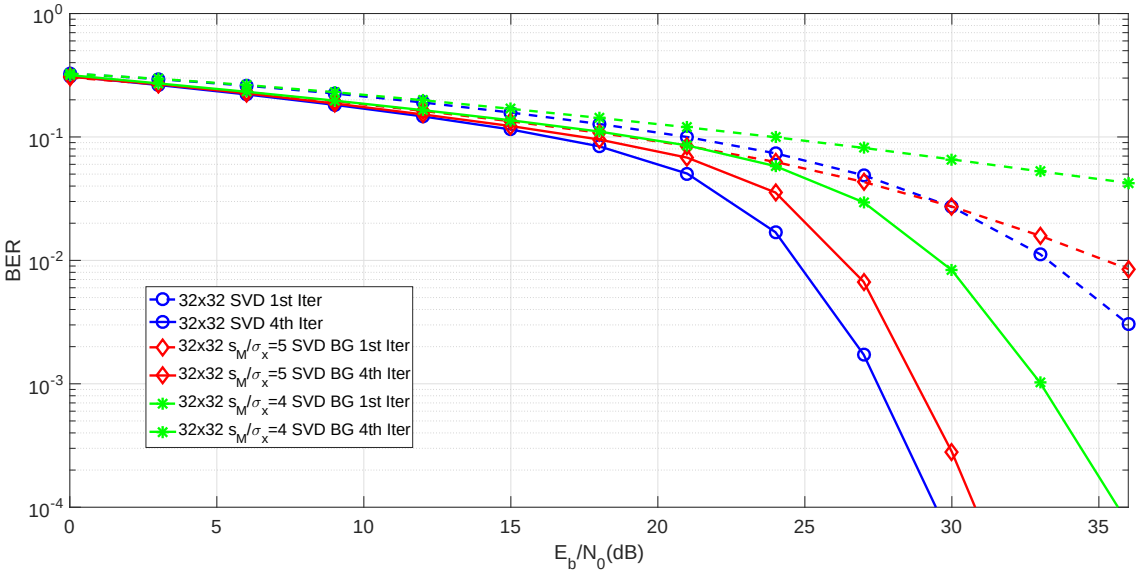

Figure 3.15: BER for a $R = T = 32$ MIMO SVD system with Bussgang cancelling, employing 64-QAM, for various clipping levels.

clipping levels as the coded receiver can withstand more distortion. We see in fig. 3.16 that the addition of the APP decoder makes this receiver's performance greatly surpass the linear receiver. Even with a clipping level of $s_M/\sigma_x = 2$, the coded receiver outperforms the non-distorted linear receiver. As is expected, we observe a sudden drop in the BER, as opposed to the smoother transition of the linear receiver, and our iterative gain is smaller as the decoder improves the results of the first iteration. For the higher modulation of 64-QAM, in fig. 3.18, the performance increase is even larger, due to the larger noise and non-linear sensitivity of this receiver. The same sharp drop and smaller iterative gain from the lower order system are observed in this figure, though happening at higher SNRs.

Next, we look at the distortion cancelling receiver in fig. 3.17. With the same clipping levels as before, we observe that the distortion cancelling receiver can outperform the linear receiver by about 4 dBs, for a BER of 10^{-4}, resulting in a performance that is much closer to a non-distorted receiver. The change in the LLR calculation of this receiver results in a better performing first iteration, that still does not have any cancellation, and, for these clipping levels, removes the iteration degradation at low SNRs that was present in the linear receivers. The iterative gain in this receiver is also larger than the linear receiver, as expected due to the nonlinear distortion cancelling of subsequent iterations.

Simlarly, for the higher order modulation in fig. 3.19, we have a substantial performance increase of about 8 dB, for a BER of 10^{-4}. There is a much more noticeable performance difference in using modulation due to the higher sensitivity of the system, which allows for a much higher boost when cancelling the distortion in the following iterations, visible in the large performance difference between iterations when compared to the 16-QAM distortion cancelling system. Likewise, for these clipping levels, the iterations never degrade performance at low SNRs due to taking into account the non-linear noise distortion power.

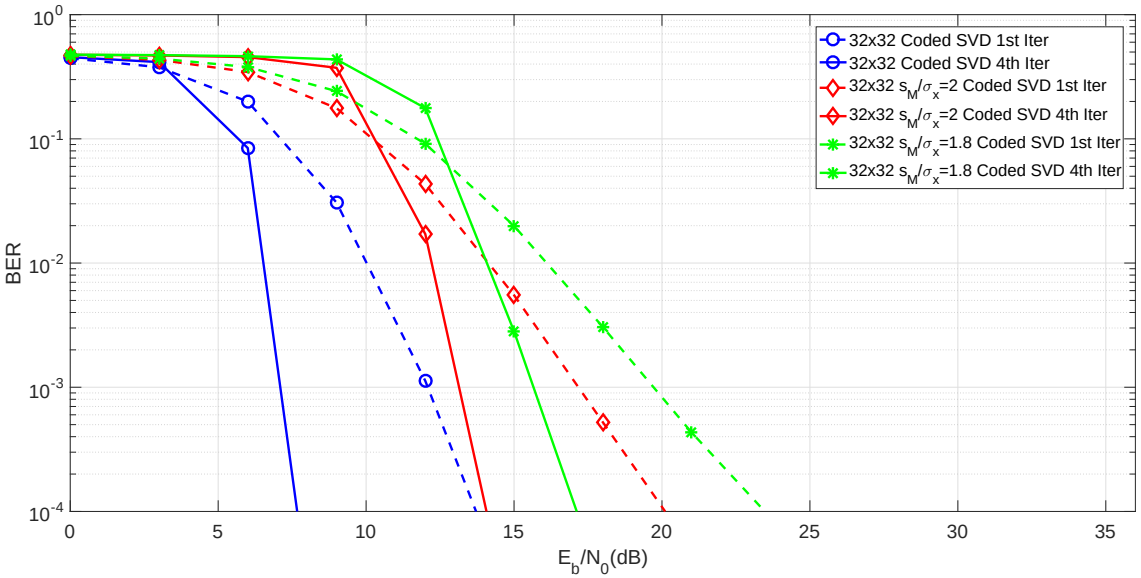

Figure 3.16: BER for a $R = T = 32$ MIMO Coded SVD system employing 16-QAM, with various clipping levels.

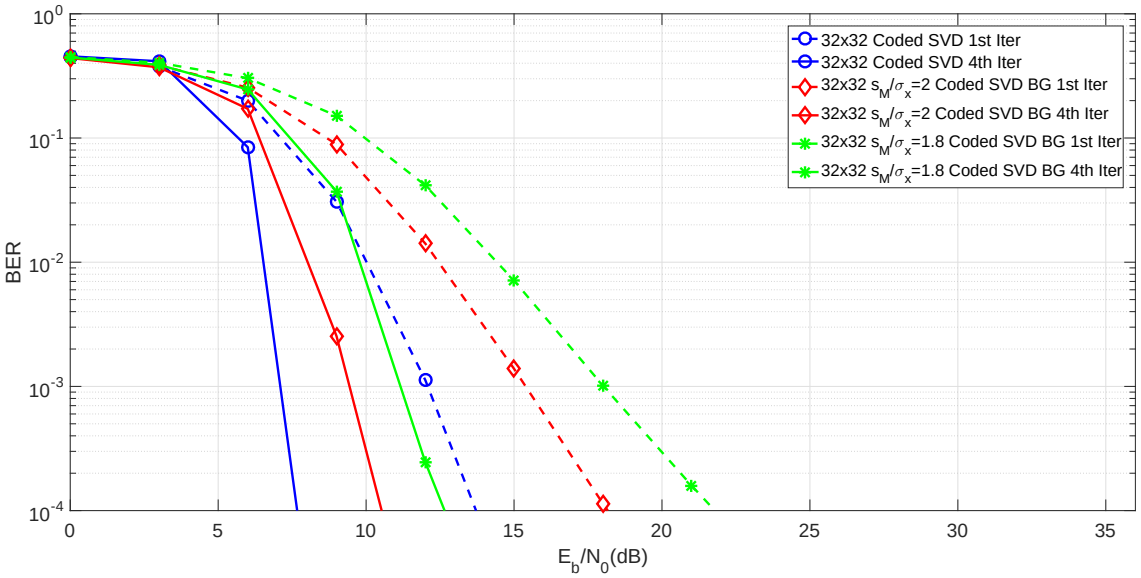

Figure 3.17: BER for a $R = T = 32$ MIMO Coded SVD system with Bussgang cancelling, employing 16-QAM, with various clipping levels.

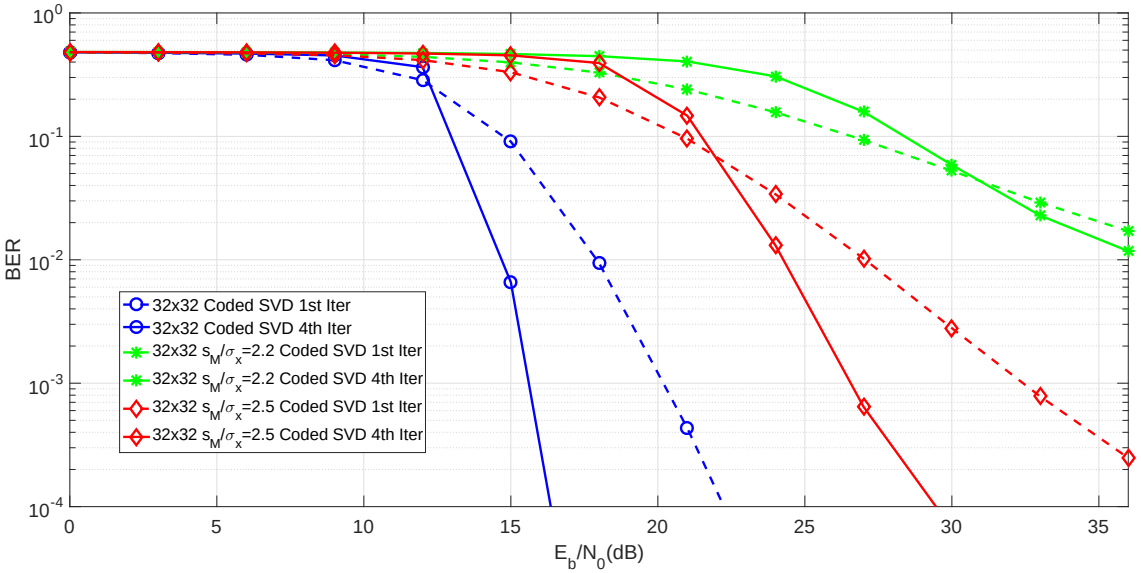

Figure 3.18: BER for a $R = T = 32$ MIMO Coded SVD system employing 64-QAM, with various clipping levels.

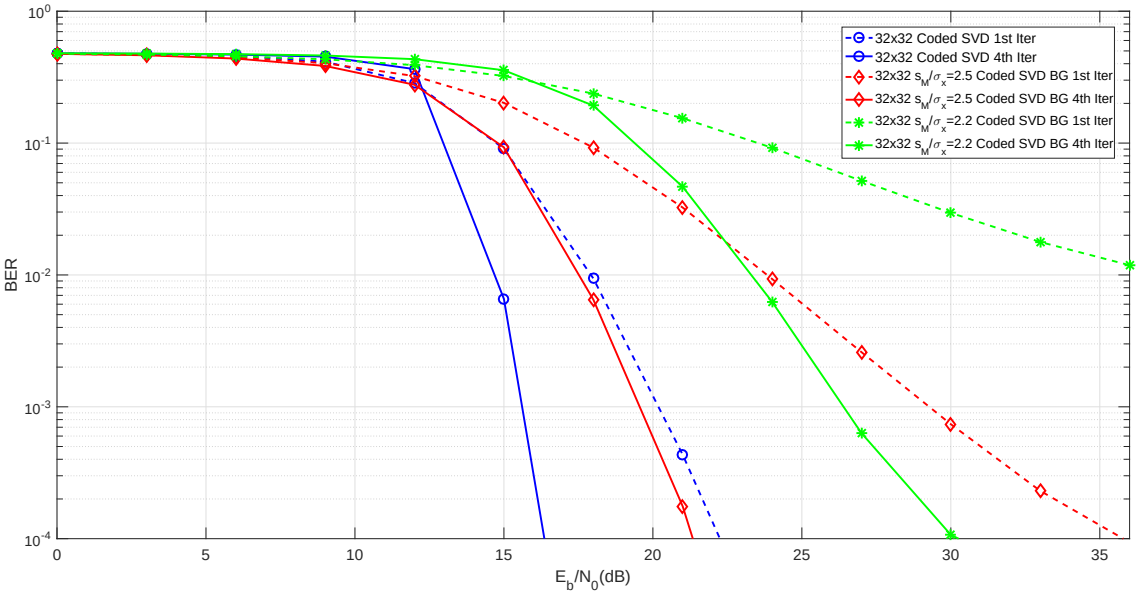

Figure 3.19: BER for a $R = T = 32$ MIMO Coded SVD system with Bussgang cancelling, employing 64-QAM, with various clipping levels.

Chapter 4

Security in Massive MIMO

4.1 Introduction

In this chapter, we present our three user scenario based on a point-to-point mMIMO Time Division Duplexing (TDD) system, where a transmitter, A, communicates with a receiver, B, and a third user, E, attempts to eavesdrop the communication. Firstly we characterize the system and channel estimates and then apply the SVD technique from Sec. 3.4 to increase the secrecy of the communications.

4.2 System

This system is comprised of a single carrier transmitter employing T transmitting antennas to send C QPSK symbol blocks of N symbols to an intended receiver, which in turn has R receiving antennas and employs an IB-DFE scheme. To separate the different streams, the transmitter and receiver employ an SVD technique. At the same time, an eavesdropper is attempting to listen to the communication. The eavesdropper also employs the SVD and IB-DFE techniques. Fig. 4.1 illustrates the system and identifies the channels considered for this system.

In Sec. 3.4 we assumed perfect knowledge of the channel, however, in this section we will use imperfect CSI. The sender and receiver will exchange pilot sequences, which will be listened by the eavesdropper, leading to different channel estimates.

4.2.1 Transmitter

Before the transmitter can apply the precoding process, it must know the channel between it and the receiver. Since the channel estimation is not perfect, we will instead define an

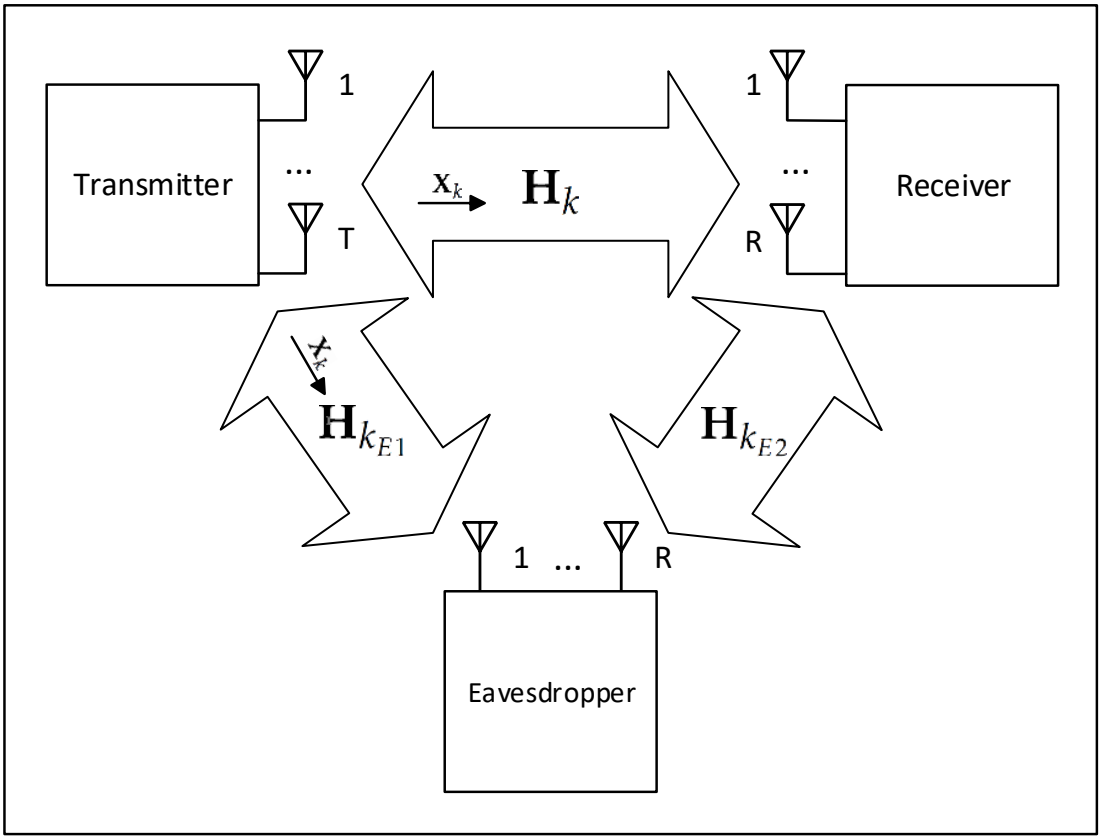

Figure 4.1: Diagram of the system with the considered channels.

equivalent channel matrix, as in [43], as

$$\mathbf{H}_k = \rho_A \hat{\mathbf{H}}_{k_A} + \boldsymbol{\epsilon}_k, \tag{4.1}$$

where $\hat{\mathbf{H}}_{k_A}$ is the channel estimate of the transmitter, ρ_A is a correlation factor between the real channel and the estimate, and $\boldsymbol{\epsilon}_k$ is the error from the channel estimation. This error $\boldsymbol{\epsilon}_k$ is characterized by complex valued Gaussian distribution with variance $2\sigma_N^2/\beta$, where σ_N^2 is the noise variance for a specific SNR, and β is a scaling factor. For $\beta \to \infty$ and $\rho_A = 1$, we have $\mathbf{H}_{k_A} = \hat{\mathbf{H}}_{k_A}$.

We write the SVD decomposition of this channel estimate as

$$\hat{\mathbf{H}}_{k_A} = \hat{\mathbf{U}}_{k_A} \hat{\boldsymbol{\Lambda}}_{k_A} \hat{\mathbf{V}}_{k_A}^H, \tag{4.2}$$

and a precoding operation as

$$\mathbf{X}'_k = \hat{\mathbf{V}}_k \mathbf{S}'_k. \tag{4.3}$$

4.2.2 Receiver

For the receiver, likewise, we define an equivalent channel as

$$\mathbf{H}_k = \rho_B \hat{\mathbf{H}}_{k_B} + \boldsymbol{\epsilon}_k, \tag{4.4}$$

where $\hat{\mathbf{H}}_{k_B}$ is the channel estimate of the receiver, and ρ_B is the correlation coefficient between the estimated and the real channel. We define an SVD operation on the channel estimate as

$$\hat{\mathbf{H}}_{k_B} = \hat{\mathbf{U}}_{k_B} \hat{\mathbf{\Lambda}}_{k_B} \hat{\mathbf{V}}^H_{k_B}. \tag{4.5}$$

It should be noted that the eavesdropper does not know the channel between the transmitter and the receiver. It only knows the channels between A and E, and between B and E. To improve the estimate, the eavesdropper averages the estimates obtained from the eavesdropped training sequences between A and B. We define three phases in this system, described graphically in fig. 4.2. First, the intended receiver sends a training sequence meant for the transmitter, which is also overheard through a different channel by the eavesdropper. In the second phase the transmitter sends a training sequence to the receiver, likewise, it is also overheard by the eavesdropper. The last phase is when the transmitter can send data blocks to the receiver, which are also received by the eavesdropper. In this phase all three users have the necessary estimations obtained from the training sequences and can perform their respective precoding and decoding operations.

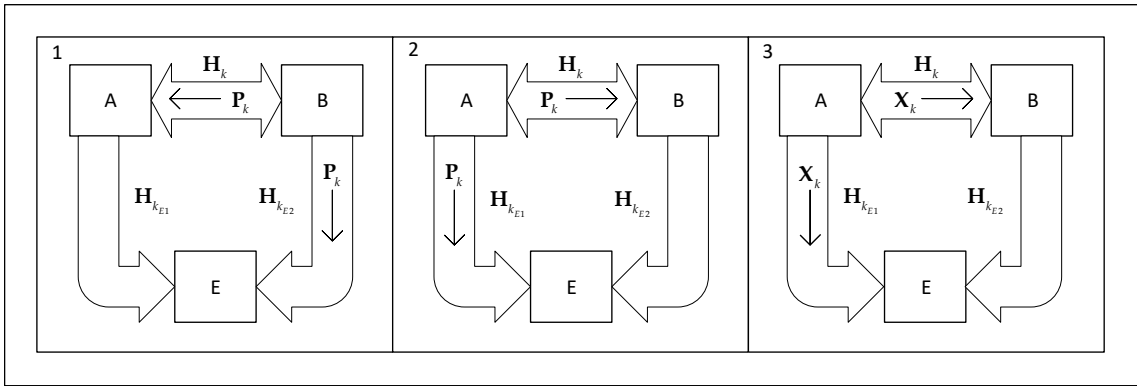

Figure 4.2: Diagram of system operation. 1) The receiver sends a training sequence. 2) The transmitter sends a training sequence. 3) The transmitter begins sending data to the receiver

We define the equivalent channels as

$$\mathbf{H}_{k_{E1}} = \rho_{E1} \hat{\mathbf{H}}_{k_{E1}} + \boldsymbol{\xi}_k + \boldsymbol{\epsilon}_k \tag{4.6}$$

and

$$\mathbf{H}_{k_{E2}} = \rho_{E2} \hat{\mathbf{H}}_{k_{E2}} + \boldsymbol{\xi}_k + \boldsymbol{\epsilon}_k, \tag{4.7}$$

with the equivalent channel as

$$\mathbf{H}_k = \frac{\mathbf{H}_{k_{E1}} + \mathbf{H}_{k_{E2}}}{2}. \tag{4.8}$$

where ρ_{E1} and ρ_{E2} are correlation factors with the real channel, and $\boldsymbol{\xi}_k$ is an error term that follows a Gaussian distribution with a variance of σ_N^2/β_M, where β_M is a scaling factor. Since the eavesdropper does not know the channel, it's not unreasonable to assume $\rho_{E1} =$

$\rho_{E2} < 1$. The decoding process is now defined for both the receiver and the eavesdropper as

$$\mathbf{W}'_k = \hat{\mathbf{U}}_k^H \mathbf{Z}'_k. \tag{4.9}$$

With the decoding complete, the deinterleaving and equalization are performed as described in the previous chapter.

Fig. 4.3 presents the BER of the intended receiver and the eavesdropper, at various ρ_E levels. As expected, the eavesdropper's BER increases with lower ρ_E values, thereby illustrating how CSI is crucial in SVD-based systems, and can be employed to increase security.

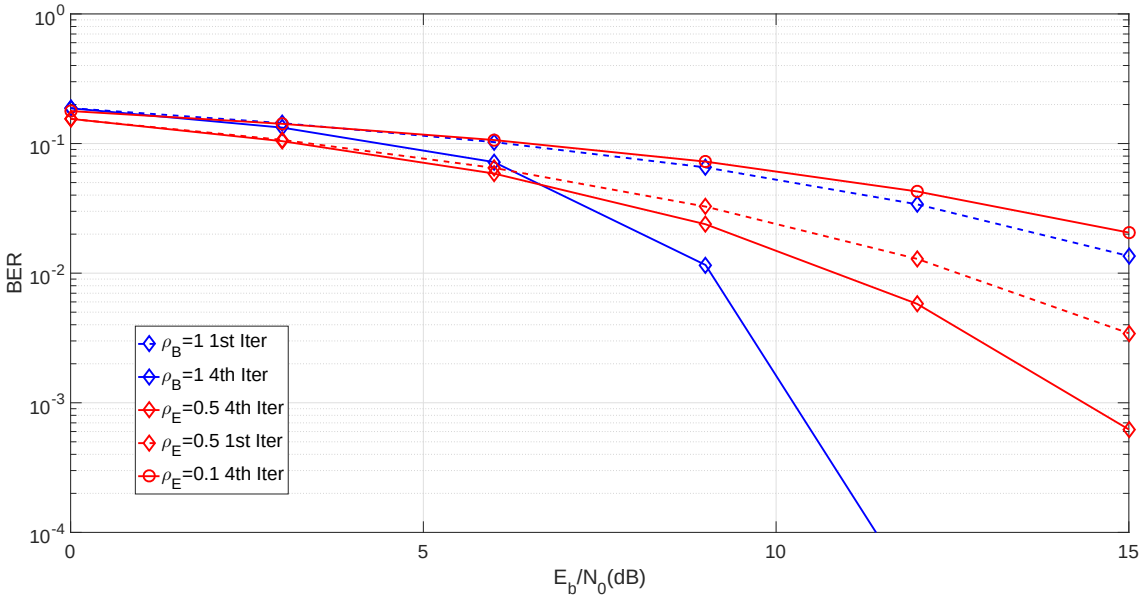

Figure 4.3: BER comparison between the intended receiver and the eavesdropper, for various values of ρ_E. Obtained for 100 blocks of 256 symbols, in a channel with Rayleigh fading.

4.3 Secrecy Rate

The SCR is defined in [32] as the difference between the capacity of the transmitter-receiver system, and the transmitter-eavesdropper system. The capacity of a fading MIMO channel is defined in [44] as

$$C = I(\mathbf{X}_k, \mathbf{Z}_k), \tag{4.10}$$

with $I(\mathbf{X}_k, \mathbf{Z}_k)$ being the mutual information between the transmitted signal, and the received signal. It is defined as

$$I(\mathbf{X}_k, \mathbf{Z}_k) = H(\mathbf{Z}_k) - H(\mathbf{Z}_k|\mathbf{X}_k), \tag{4.11}$$

with $H(\mathbf{Z}_k)$ being the differential entropy of $\mathbf{Z}_k$ and $H(\mathbf{Z}_k|\mathbf{X}_k)$ the conditional differential entropy of $\mathbf{Z}_k$ given $\mathbf{X}_k$. Since we know that $\mathbf{X}_k$ is independent of $\mathbf{N}_k$, we can simplify

$H(\mathbf{Z}_k|\mathbf{X}_k) = H(\mathbf{N}_k)$. The differential entropies are given by

$$H(\mathbf{Z}_k) = \log_2((\pi e)^{\sigma_N^2} \det(\mathbf{H}_k \mathbf{R}_X \mathbf{H}_k^H + \mathbf{R}_N)), \tag{4.12}$$

and

$$H(\mathbf{N}_k) = \log_2((\pi e)^{\sigma_N^2} \det(\mathbf{R}_N)), \tag{4.13}$$

where $\mathbf{R_X} = \sigma_X^2 \mathbf{I}$ and $\mathbf{R_N} = \sigma_N^2 \mathbf{I}$, with σ_X^2 and σ_N^2 corresponding to the variances of $\mathbf{X}_k$ and $\mathbf{N}_k$, respectively. With the entropies defined we can expand (4.11) and simplify into:

$$\begin{aligned} I(\mathbf{X}_k, \mathbf{Z}_k) &= H(\mathbf{Z}_k) - H(N_k) \\ &= \log_2(det(\mathbf{H}_k \mathbf{R}_X \mathbf{H}_k^H + \mathbf{R}_N)\mathbf{R}_N^{-1}) \\ &= \log_2(det(\mathbf{I} + \mathbf{H}_k \mathbf{H}_k^H \frac{\sigma_X^2}{\sigma_N^2})) \\ &= \log_2(det(\mathbf{I} + |\mathbf{\Lambda}_k|^2 SNR)) \\ &= \sum_{i=0}^{C} \log_2(1 + |\lambda_i|^2 SNR). \end{aligned} \tag{4.14}$$

Since we have two different transmitter-receiver pairs, we can, likewise, define two different system capacities. First, we define the capacity of the system with the intended receiver, that is A to B, as

$$C_{AB} = \sum_{i=0}^{C} \log_2(1 + |\lambda_i \rho_B|^2 \frac{\sigma_X^2}{\sigma_N^2 + \sigma_B^2}), \tag{4.15}$$

where σ_X^2 is the corresponding variance of the received signal, σ_N^2 is the noise variance at the receiver and σ_B^2 is the interference power due to the imperfect channel estimation, defined as

$$2\sigma_B^2 = \mathbb{E}[\hat{\mathbf{\Lambda}}_{k_B}^I \hat{\mathbf{\Lambda}}_{k_B}^{IH}], \tag{4.16}$$

with $\hat{\mathbf{\Lambda}}_{k_B}^I$ denoting a matrix comprised of the interference in the receiver, computed as

$$\hat{\mathbf{\Lambda}}_{k_B}^I = \hat{\mathbf{\Lambda}}_{k_B} - \text{diag}(\hat{\mathbf{\Lambda}}_{k_B}). \tag{4.17}$$

Similarly for the eavesdropper, we can define the capacity of the link between A and E as

$$C_{AE} = \sum_{i=0}^{C} log_2(1 + |\lambda_{i_E} \rho_E|^2 \frac{\sigma_X^2}{\sigma_N^2 + \sigma_E^2}) \tag{4.18}$$

where ρ_E is a simplification defined as $\rho_E = \rho_{E1} = \rho_{E2}$, and σ_E^2 is the interference power due to the imperfect channel estimation, which is larger than σ_B, and is computed as

$$2\sigma_E^2 = \mathbb{E}[\hat{\mathbf{\Lambda}}_{k_E}^I \hat{\mathbf{\Lambda}}_{k_E}^{IH}]. \tag{4.19}$$

Likewise, $\hat{\mathbf{\Lambda}}_{k_E}^I$ is the interference matrix computed as

$$\hat{\mathbf{\Lambda}}_{k_E}^I = \hat{\mathbf{\Lambda}}_{k_E} - \text{diag}(\hat{\mathbf{\Lambda}}_{k_E}). \tag{4.20}$$

By taking into account the capacities defined in (27) and (30), we can compute the secrecy rate as

$$SR = C_{AB} - C_{AE}. \tag{4.21}$$

4.4 Performance

For verifying the SCR of this system, we used Monte-Carlo simulations over 100 blocks of 256 symbols, over a channel characterized by a Rayleigh distribution. Firstly, we examine the impact of a channel estimation error with the same power in all three users, in fig. 4.4. For lower errors in the CSI and lower ρ_E, we obtain a higher SCR. If we take into account that the eavesdropper will have an additional error, due to not being able to know the channel between A and B, then we can achieve a higher maximum SCR, as shown in fig. 4.5. Lastly, we measure the impact of the SNR on the SCR in fig. 4.6. For higher SNR levels, we achieve a higher SCR.

In conclusion, in order to maximise the SCR we can minimise the error in the CSI, by using more efficient channel estimation methods. Although increasing transmit power would also increase the SCR, this is usually not practical in mobile systems, but may be interesting in other types of systems, that have higher power constraints. It is usually not necessary to maximise the error in the eavesdropper in mm-Wave communications, as even a distance of 1m is already several times larger than the wavelength.

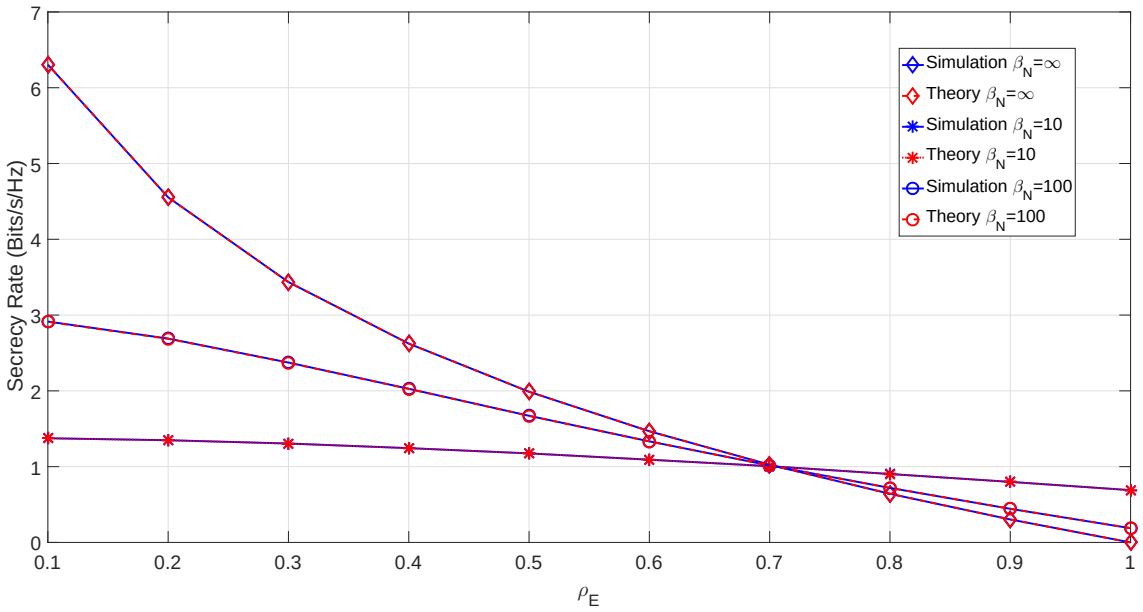

Figure 4.4: SCR for various levels of β_N at 12 dB.

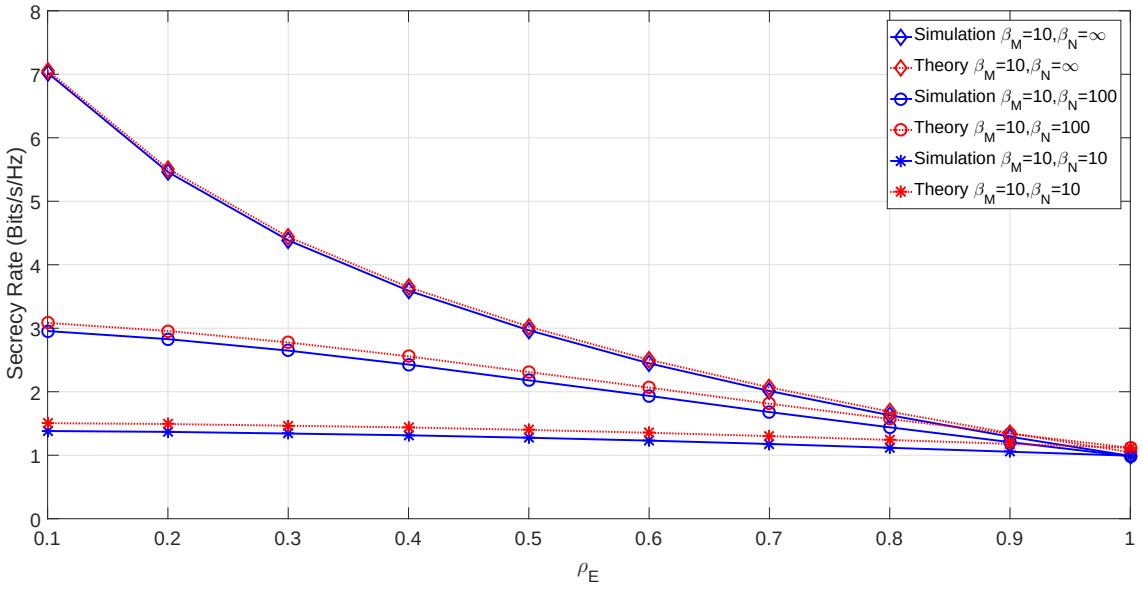

Figure 4.5: SCR for various levels of β_N, with $\beta_M = 10$ at 12dB.

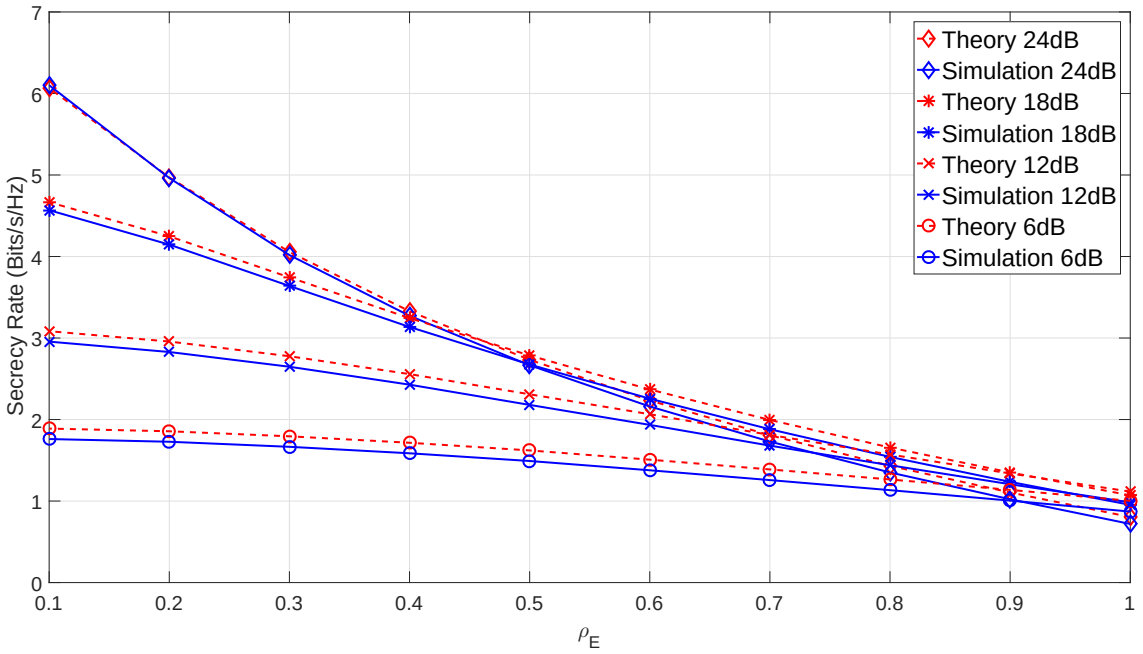

Figure 4.6: SCR for various SNR levels with $\beta_N = 100$ and $\beta_M = 10$.

4.5 Communication with Line-of-Sight Links

Another possible scenario is the one where there is a direct Line-of-Sight (LoS) between the transmitter and both the receiver and eavesdropper. Under these conditions the channel is defined as the sum of an LoS low fading component, and several uncorrelated multipath rays with high fading. We admit that the eavesdropper can only estimate the LoS component with a certain error, and cannot estimate the remaining multipath rays. In this case we define the channel as

$$\mathbf{H}_{k,los} = \mathbf{D}_{k_{los}} + \mathbf{R}_{k_{mp}}, \tag{4.22}$$

where $\mathbf{D}_{k_{los}}$ is the low fading high correlation component and $\mathbf{R}_{k_{mp}}$ is the high fading multipath component of the channel. We then substitute this channel in (4.1) and (4.4), as

$$\mathbf{H}_{k,los} = \rho_A \hat{\mathbf{H}}_{k_A} + \boldsymbol{\epsilon}_k, \tag{4.23}$$

$$\mathbf{H}_{k,los} = \rho_B \hat{\mathbf{H}}_{k_B} + \boldsymbol{\epsilon}_k. \tag{4.24}$$

The intended receiver and transmitter's remaining operations are calculated as described previously.

The eavesdropper, however, cannot estimate the multipath component of the channel, and must instead rely on the estimate of the LoS component. We define this component as

$$\mathbf{D}_{k_{los}} = \frac{\mathbf{H}_{k_{E1,los}} + \mathbf{H}_{k_{E2,los}}}{2}, \tag{4.25}$$

where

$$\mathbf{H}_{k_{E1,los}} = \rho_{E1} \hat{\mathbf{H}}_{k_{E1,los}} + \xi_k + \boldsymbol{\epsilon}_k \tag{4.26}$$

and

$$\mathbf{H}_{k_{E2,los}} = \rho_{E2} \hat{\mathbf{H}}_{k_{E2,los}} + \xi_k + \boldsymbol{\epsilon}_k. \tag{4.27}$$

In this scenario, the channel estimates $\hat{\mathbf{H}}_{k_{E1,los}}$ and $\hat{\mathbf{H}}_{k_{E2,los}}$ are of only the LoS component between A and E, and B and E, respectively. The difference between these estimates and the real channel will be proportional to the power of the multipath component. If this component corresponds to 0% of the channel power, then the channel is composed of only the LOS component , whereas at 100% power the channel is composed of only the multipath component.

We then performed simulations under the same conditions as the previous scenario and analyse the results.In Fig. 4.7 it is observed that the higher the ray power ratio, the higher the achievable secrecy rate. This is expected, since the component that the eavesdropper can estimate contributes less to the total channel power. In the noisy CSI, scenario we have similar results, as shown in Fig. 4.8. The unknown multipath component introduces a permanent error in the eavesdropper, which accounts for the higher

SCR at $\rho_E = 1$, similar to the mismatch error. If we add the mismatch error as well, we observe in fig. 4.9 the same as effect as in the previous scenario, where there is a significant increase in the SCR only for higher values of ρ_E.

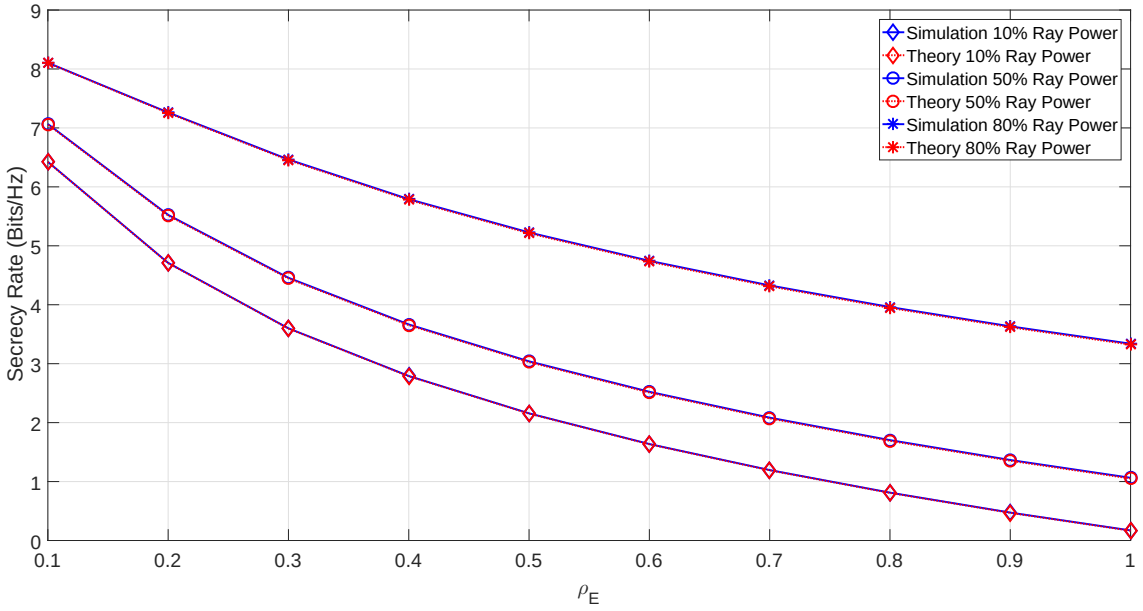

Figure 4.7: SCR for various ray power ratios with $\beta_N = \infty$.

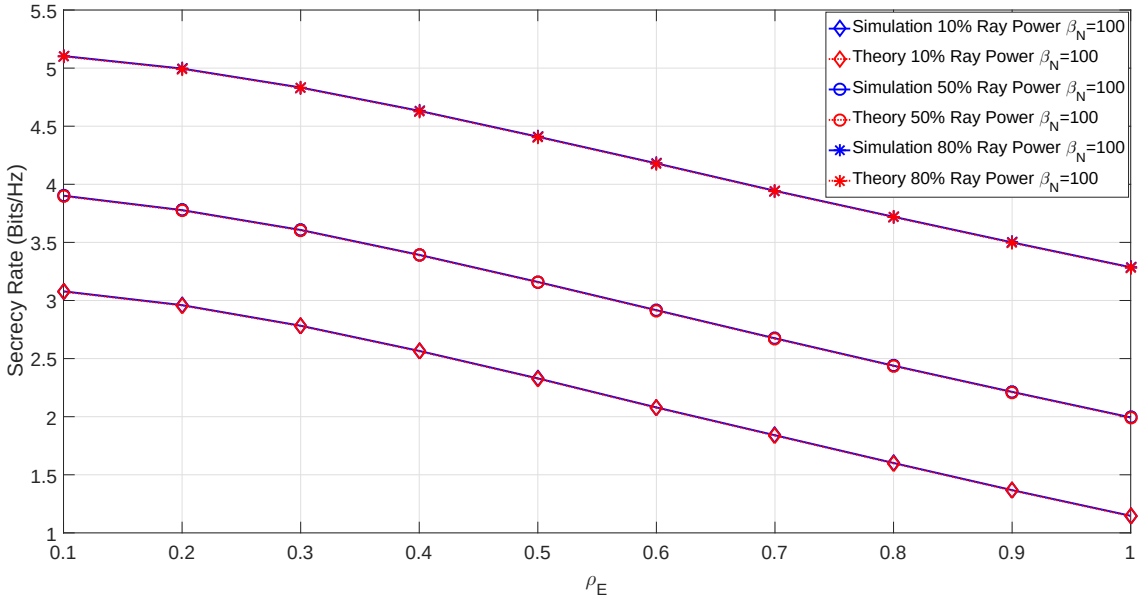

Figure 4.8: SCR for various ray power ratios with $\beta_N = 100$ at 12dB SNR.

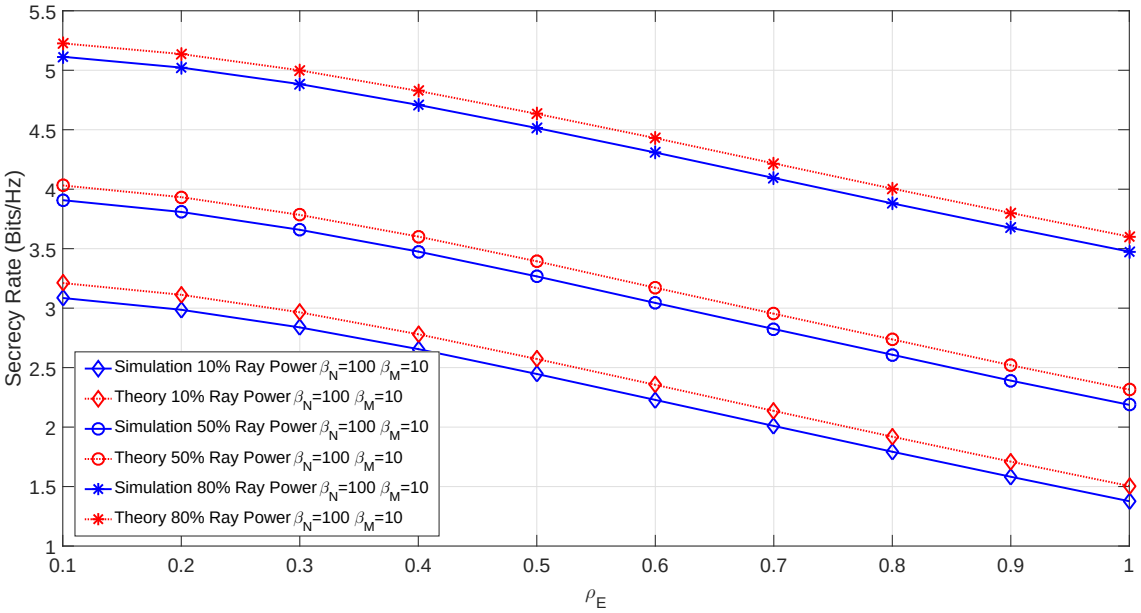

Figure 4.9: SCR for various ray power ratios with $\beta_N = 100$ and $\beta_M = 10$ at 12dB SNR.

Chapter 5

Conclusions and Final Remarks

5.1 Conclusions

The main goal of this work was to study different types of MIMO receivers, each with a different trade-off, and how could they perform in various situations and configurations. We began in Chapter 2 by introducing classical SC MIMO systems, and what advantages and disadvantages they brought over their SISO counterparts. As we demonstrated, these traditional systems may not be viable for mMIMO configurations due to various reasons, which motivated the study of the proposed alternative receivers.

In Chapter 3, we studied receivers with a focus on efficiency. The first set of receivers, the EGD and MRD, were studied due to their low complexity for large antenna arrays. These receivers are particularly interesting for uplink scenarios, when the BS has more antennas than the number of MTs, as the reduced complexity results in smaller processing time per block, which in turn leads to lower delays.

In the next section, we analysed a receiver focused on increasing energy efficiency, the Bussgang SVD. This receiver can withstand smaller clipping levels than the linear receiver, which makes it appealing for systems that want to prioritise energy consumption. However, this receiver cannot be characterized as either uplink or downlink, as it is a point-to-point communication. It is therefore difficult to integrate this receiver in a mobile network scenario, unless we're assuming a scenario with a communication between two BSs or similar, but does make it interesting for satellite communications.

Since we are analysing efficient receivers, we must also discuss coding. We employed a simple but powerful code on all receivers and confirmed the expected large performance gain that makes coding an essential component of any telecommunication system.

Efficiency is not the only requirement of newer systems, with security becoming increasingly more important in modern days. As such, we analysed the security potential

of SVD systems. Since this system operates as a point-to-point system, where there are only two users involved, it achieves very favourable results due to its eavesdropping difficulty. However, these results require very efficient channel estimation schemes, which may introduce other downsides to the system.

5.2 Main Contributions

The work developed in this dissertation has also been published in [45] and [46], and one currently submitted paper.

5.3 Future Work

Although the receivers show positive results, there is still room for improvement. Particularly the bussgang receiver can still be improved by using more powerful error correcting codes, such as LDPC, or by implementing a different solution altogether that can take advantage of the non-linearity to improve performance, such as Generalised Approximate Message Passing (GAMP) which is still undergoing initial studying. The security aspect of this receiver can also be greatly improved by using higher performance channel estimation methods, such as joint channel detection. These techniques would make it harder for an eavesdropper to listen, and improve the quality of the channel estimate.

Bibliography

[1] C. E. Shannon. "A mathematical theory of communication." In: *Bell system technical journal* 27.3 (1948), pp. 379–423.

[2] C. Lange, D. Kosiankowski, R. Weidmann, and A. Gladisch. "Energy Consumption of Telecommunication Networks and Related Improvement Options." In: *IEEE Journal of Selected Topics in Quantum Electronics* 17.2 (2011), pp. 285–295. ISSN: 1077-260X. DOI: 10.1109/JSTQE.2010.2053522.

[3] *Sustainable Business Report 2017*. Tech. rep. Vodafone Group Plc, 2017.

[4] F. Boccardi, R. W. Heath, A. Lozano, T. L. Marzetta, and P. Popovski. "Five disruptive technology directions for 5G." In: *IEEE Communications Magazine* 52.2 (2014), pp. 74–80. ISSN: 0163-6804. DOI: 10.1109/MCOM.2014.6736746.

[5] D. J. Love, R. W. Heath, and T. Strohmer. "Grassmannian beamforming for multiple-input multiple-output wireless systems." In: *IEEE International Conference on Communications, 2003. ICC '03.* Vol. 4. 2003, 2618–2622 vol.4. DOI: 10.1109/ICC.2003.1204421.

[6] D. Falconer, S. L. Ariyavisitakul, A. Benyamin-Seeyar, and B. Eidson. "Frequency domain equalization for single-carrier broadband wireless systems." In: *IEEE Communications Magazine* 40.4 (2002), pp. 58–66. ISSN: 0163-6804. DOI: 10.1109/35.995852.

[7] N. Benvenuto and S. Tomasin. "Block iterative DFE for single carrier modulation." In: *Electronics Letters* 38.19 (2002), pp. 1144–1145. ISSN: 0013-5194. DOI: 10.1049/el:20020767.

[8] N. Benvenuto and S. Tomasin. "Iterative design and detection of a DFE in the frequency domain." In: *IEEE Transactions on Communications* 53.11 (2005), pp. 1867–1875. ISSN: 0090-6778. DOI: 10.1109/TCOMM.2005.858666.

[9] R. Dinis, P. Montezuma, N. Souto, and J. Silva. "Iterative Frequency-Domain Equalization for general constellations." In: *2010 IEEE Sarnoff Symposium*. 2010, pp. 1–5. DOI: 10.1109/SARNOF.2010.5469792.

[10] C. E. Shannon. "Communication in the Presence of Noise." In: *Proceedings of the IRE* 37.1 (1949), pp. 10–21. ISSN: 0096-8390. DOI: 10.1109/JRPROC.1949.232969.

[11] J. H. Van Lint. *Introduction to coding theory*. Vol. 86. Springer Science & Business Media, 2012.

[12] R. Johannesson and K. S. Zigangirov. *Fundamentals of convolutional coding*. Vol. 15. John Wiley & Sons, 2015.

[13] L. Bahl, J. Cocke, F. Jelinek, and J. Raviv. "Optimal decoding of linear codes for minimizing symbol error rate (Corresp.)" In: *IEEE Transactions on Information Theory* 20.2 (1974), pp. 284–287. ISSN: 0018-9448. DOI: 10.1109/TIT.1974.1055186.

[14] T. Richardson. "Error floors of LDPC codes." In: *Proceedings of the annual Allerton conference on communication control and computing*. Vol. 41. 3. The University; 1998. 2003, pp. 1426–1435.

[15] C. Berrou, A. Glavieux, and P. Thitimajshima. "Near Shannon limit error-correcting coding and decoding: Turbo-codes. 1." In: *Proceedings of ICC '93 - IEEE International Conference on Communications*. Vol. 2. 1993, 1064–1070 vol.2. DOI: 10.1109/ICC.1993.397441.

[16] L. Lu, G. Y. Li, A. L. Swindlehurst, A. Ashikhmin, and R. Zhang. "An Overview of Massive MIMO: Benefits and Challenges." In: *IEEE Journal of Selected Topics in Signal Processing* 8.5 (2014), pp. 742–758. ISSN: 1932-4553. DOI: 10.1109/JSTSP.2014.2317671.

[17] E. G. Larsson, O. Edfors, F. Tufvesson, and T. L. Marzetta. "Massive MIMO for next generation wireless systems." In: *IEEE Communications Magazine* 52.2 (2014), pp. 186–195. ISSN: 0163-6804. DOI: 10.1109/MCOM.2014.6736761.

[18] F. G.J. and G. M.J. "On Limits of Wireless Communications in a Fading Environment when Using Multiple Antennas." In: *Wireless Personal Communications* 6.3 (1998), pp. 311–335. ISSN: 1572-834X. DOI: 10.1023/A:1008889222784. URL: https://doi.org/10.1023/A:1008889222784.

[19] A. Goldsmith. *Wireless communications*. Cambridge university press, 2005.

[20] P. W. Wolniansky, G. J. Foschini, G. D. Golden, and R. A. Valenzuela. "V-BLAST: an architecture for realizing very high data rates over the rich-scattering wireless channel." In: *1998 URSI International Symposium on Signals, Systems, and Electronics. Conference Proceedings (Cat. No.98EX167)*. 1998, pp. 295–300. DOI: 10.1109/ISSSE.1998.738086.

[21] L. Lu, G. Y. Li, A. L. Swindlehurst, A. Ashikhmin, and R. Zhang. "An Overview of Massive MIMO: Benefits and Challenges." In: *IEEE Journal of Selected Topics in Signal Processing* 8.5 (2014), pp. 742–758. ISSN: 1932-4553. DOI: 10.1109/JSTSP.2014.2317671.

[22] S. Noh, M. D. Zoltowski, Y. Sung, and D. J. Love. "Pilot Beam Pattern Design for Channel Estimation in Massive MIMO Systems." In: *IEEE Journal of Selected Topics in Signal Processing* 8.5 (2014), pp. 787–801. ISSN: 1932-4553. DOI: 10.1109/JSTSP.2014.2327572.

[23] C. Wen, S. Jin, K. Wong, J. Chen, and P. Ting. "Channel Estimation for Massive MIMO Using Gaussian-Mixture Bayesian Learning." In: *IEEE Transactions on Wireless Communications* 14.3 (2015), pp. 1356–1368. ISSN: 1536-1276. DOI: 10.1109/TWC.2014.2365813.

[24] U.-K. Kwon, D. Kim, and G.-H. Im. "Amplitude clipping and iterative reconstruction of MIMO-OFDM signals with optimum equalization." In: *IEEE Transactions on Wireless Communications* 8.1 (2009), pp. 268–277.

[25] C. Risi, D. Persson, and E. G. Larsson. "Massive MIMO with 1-bit ADC." In: *arXiv preprint arXiv:1404.7736* (2014).

[26] J. Guerreiro, R. Dinis, and P. Montezuma. "Use of 1-bit digital-to-analogue converters in massive MIMO systems." In: *Electronics Letters* 52.9 (2016), pp. 778–779. ISSN: 0013-5194. DOI: 10.1049/el.2015.4037.

[27] I. Tafur Monroy. *Achieving a 90% reduction in power consumption for 5G*. Tech. rep. Bluespace 5G-PPP, 2017.

[28] G. Santella and F. Mazzenga. "A model for performance evaluation in M-QAM-OFDM schemes in prescence of nonlinear distortions." In: *1995 IEEE 45th Vehicular Technology Conference. Countdown to the Wireless Twenty-First Century*. Vol. 2. 1995, 830–834 vol.2. DOI: 10.1109/VETEC.1995.504984.

[29] M. Bloch, J. Barros, M. R. D. Rodrigues, and S. W. McLaughlin. "Wireless Information-Theoretic Security." In: *IEEE Transactions on Information Theory* 54.6 (2008), pp. 2515–2534. ISSN: 0018-9448. DOI: 10.1109/TIT.2008.921908.

[30] Y. Shiu, S. Y. Chang, H. Wu, S. C. Huang, and H. Chen. "Physical layer security in wireless networks: a tutorial." In: *IEEE Wireless Communications* 18.2 (2011), pp. 66–74. ISSN: 1536-1284. DOI: 10.1109/MWC.2011.5751298.

[31] L. Dong, Z. Han, A. P. Petropulu, and H. V. Poor. "Improving Wireless Physical Layer Security via Cooperating Relays." In: *IEEE Transactions on Signal Processing* 58.3 (2010), pp. 1875–1888. ISSN: 1053-587X. DOI: 10.1109/TSP.2009.2038412.

[32] F. Oggier and B. Hassibi. "The Secrecy Capacity of the MIMO Wiretap Channel." In: *IEEE Transactions on Information Theory* 57.8 (2011), pp. 4961–4972. ISSN: 0018-9448. DOI: 10.1109/TIT.2011.2158487.

[33] D. Borges, P. Montezuma, and R. Dinis. "Low complexity MRC and EGC based receivers for SC-FDE modulations with massive MIMO schemes." In: *2016 IEEE Global Conference on Signal and Information Processing (GlobalSIP)*. 2016, pp. 675–678. DOI: 10.1109/GlobalSIP.2016.7905927.

[34] R. Dinis and P. Montezuma. "Iterative receiver based on the EGC for massive MIMO schemes using SC-FDE modulations." In: *Electronics Letters* 52.11 (2016), pp. 972–974. ISSN: 0013-5194. DOI: 10.1049/el.2016.0012.

[35] M. Kang and M. Alouini. "A comparative study on the performance of MIMO MRC systems with and without cochannel interference." In: *IEEE Transactions on Communications* 52.8 (2004), pp. 1417–1425. ISSN: 0090-6778. DOI: 10.1109/TCOMM.2004.833027.

[36] G. Lebrun, J. Gao, and M. Faulkner. "MIMO transmission over a time-varying channel using SVD." In: *IEEE Transactions on Wireless Communications* 4.2 (2005), pp. 757–764. ISSN: 1536-1276. DOI: 10.1109/TWC.2004.840199.

[37] H. Yang and T. L. Marzetta. "Performance of Conjugate and Zero-Forcing Beamforming in Large-Scale Antenna Systems." In: *IEEE Journal on Selected Areas in Communications* 31.2 (2013), pp. 172–179. ISSN: 0733-8716. DOI: 10.1109/JSAC.2013.130206.

[38] J. Bussgang. "Crosscorrelation functions of amplitude-distorted gaussian signals." In: *M.I.T. RLE Technical Reports* 216 (1952), pp. 1–14.

[39] F. Rusek, D. Persson, B. K. Lau, E. G. Larsson, T. L. Marzetta, O. Edfors, and F. Tufvesson. "Scaling Up MIMO: Opportunities and Challenges with Very Large Arrays." In: *IEEE Signal Processing Magazine* 30.1 (2013), pp. 40–60. ISSN: 1053-5888. DOI: 10.1109/MSP.2011.2178495.

[40] A. Ahrens, C. Benavente-Peces, and A. Aboltins. "Performance comparison of SVD- and GMD-assisted MIMO systems." In: *2015 Advances in Wireless and Optical Communications (RTUWO)*. 2015, pp. 5–12. DOI: 10.1109/RTUWO.2015.7365708.

[41] J. Guerreiro, R. Dinis, and P. Montezuma. "On the Impact of Strong Nonlinear Effects on Massive MIMO SVD Systems with Imperfect Channel Estimates." In: *2017 IEEE 86th Vehicular Technology Conference (VTC-Fall)*. 2017, pp. 1–5. DOI: 10.1109/VTCFall.2017.8288010.

[42] J. F.M. L. Guerreiro. "Analytical Characterization and Optimum Detection of Nonlinear Multicarrier Schemes." Doctorate. Faculdade de Ciências e Tecnologia.

[43] J. Guerreiro, R. Dinis, and P. Montezuma. "Analytical Performance Evaluation of Precoding Techniques for Nonlinear Massive MIMO Systems With Channel Estimation Errors." In: *IEEE Transactions on Communications* 66.4 (2018), pp. 1440–1451. ISSN: 0090-6778. DOI: 10.1109/TCOMM.2017.2782321.

[44] I. E. Telatar. "Capacity of multi-antenna Gaussian channels." In: *EUROPEAN TRANSACTIONS ON TELECOMMUNICATIONS* 10 (1999), pp. 585–595.

[45] J. Madeira, J. Guerreiro, and R. Dinis. "Turbo Multi-User Detection for SC-FDE Massive MIMO Systems." In: *2018 IEEE 87th Vehicular Technology Conference (VTC Spring)*. 2018, pp. 1–5. DOI: 10.1109/VTCSpring.2018.8417584.

[46] J. Madeira, J. Guerreiro, and R. Dinis. "Iterative Frequency-Domain Detection for MIMO Systems with Strong Nonlinear Distortion Effects." In: *2018 IEEE 10th International Congress on Ultra Modern Telecommunications and Control Systems (ICUMT)*. 2018.